COMPUTATIONAL STUDY OF GRAPHENE NANOPORE SENSOR FOR DNA SENSING

BY

CHAITANYA SATHE

DISSERTATION

Submitted in partial fulfillment of the requirements
for the degree of Doctor of Philosophy in Electrical and Computer Engineering
in the Graduate College of the
University of Illinois at Urbana-Champaign, 2014

Urbana, Illinois

Doctoral Committee:

Professor Jean-Pierre Leburton, Chair
Professor Klaus Schulten
Professor Joseph Lyding
Professor Rashid Bashir

ABSTRACT

Inexpensive and fast methods to sequence the genome of individuals using nanopore technology can lead to tremendous advancement in the field of modern medicine. The thickness of the membranes employed in nanopore-based sensors presents a fundamental limitation to the physical dimension, of the translocating DNA molecule, that can be resolved. Typical solid-state membranes are too thick and usually fail to recognize single nucleotides on a DNA strand. Graphene is a sub-nanometer membrane, comprising of carbon atoms arranged in a honeycomb lattice, with remarkable electronic and mechanical properties. The thickness of a graphene membrane (3 Å) is comparable to the vertical stacking distance between base pairs in the DNA (3.5 Å) making graphene an ideal candidate for DNA sequencing. Resolving at the atomic level electric field-driven DNA translocation through graphene nanopores is crucial to guide the design of graphene-based sequencing devices. Molecular dynamics (MD) simulations, in principle, can achieve such resolution and are employed to investigate the effects of applied voltage, DNA conformation and sequence as well as pore charge on the translocation characteristics of DNA. In addition, graphene is electrically active and transverse electronic currents along the graphene membrane can complement ionic current measurements, and potentially extend the molecular sensing capability of graphene-based nanopores. We have combined the self-consistent Poisson-Boltzmann formalism with Non-Equilibrium Green's Function (NEGF) technique along with charge densities of DNA arising from MD simulations to show detection of rotational and positional conformation of a double-stranded DNA (dsDNA), inside the nanopore, via sheet currents in graphene nanoribbons. Furthermore, we show the ability of such transverse electronic currents to detect conformational transition, arising due to forced extension, of the dsDNA molecule from helical to zipper form, and also detect ssDNA translocation at single base pair resolution.

To Aiye (Mother) and Dadda (Father)

ACKNOWLEDGMENTS

This work was supported by grants 9P41GM104601 from the National Institute of Health (NIH) and PHY0822613 from the National Science Foundation (NSF). The author also acknowledges Beckman Institute for a graduate fellowship. Supercomputer time was provided through the Texas Advanced Computing Center via the Extreme Science and Engineering Discovery Environment (XSEDE) grant, which is supported by NSF grant number OCI-1053575. The author also acknowledges the use of the parallel computing resource Taub provided by the Computational Science and Engineering Program at the University of Illinois.

There are many people who have helped and supported me during my graduate study at the University of Illinois Urbana-Champaign. I would like to thank Klaus Schulten and Jean-Pierre Leburton for guiding me through my research and helping me to choose the current thesis topic. Klaus has nurtured students to think independently and always encouraged me to explore my interests and ideas. His infectious enthusiasm for science, penchant for perfection, and broad scientific vision have been a great source of inspiration. Klaus provided me with valuable advice and criticism, when I needed it and has taught me how to write and present scientific discoveries. I consider myself very fortunate to have had the opportunity to work with him and the Theoretical and Computational Biophysics Group (TCBG). I would like to express my thanks to Jean-Pierre who has been instrumental in shaping my research project and keeping me on track. Jean-Pierre has also taught me about semiconductor transport and TAing his course has been an enriching experience for me. He always made himself easily accessible to his students, the research project has benefitted a lot from Jean-Pierre's enthusiasm and expertise. I would also like to thank Prof. Joseph Lyding and Prof. Rashid Bashir for serving on my prelim and defense committees. My heartfelt thanks

to Prof. Mahesh Patil (EE IITB) who has been a role model and constantly reminds me of the positive influence people in academia can have on students.

Many thanks to Anuj Girdhar and Xueqing Zou who have been wonderful collaborators. I would like to also thank Jim, John, Kirby and Haley for providing leading-edge facilities to carry out research. Many thanks to Wen, Keith, Boon, and Juan for their companionship. Wen has been a wonderful officemate, I will cherish the endless discussions we had on science, politics and general gossip, not to forget his sarcasm and good sense of humor. I would be remiss in forgetting Yanxin Liu, Lela Vukovic, Wei Han, Rafael Bernardi, Till Rudack, Melih Sener, Barry Isralewitz, Zhe Wu, Angela Barrangan, Yan Chan, Rezvan Shahoei, Ilia Solovyov, Danielle Chandler, David Hardy, Ryan Mc Greevy, Maxim Belkin, Ramya Gamini, Jen Hsin, Bo Liu, Kin Lam, Hang Yu, Ivan Teo, Yi Zhang, Johan Strumpfer, J. C. Gumbart, Eric Lee, Eduardo Cruz Chu and Abhi Singharoy.

Special thanks to Nancy Mellon, who perhaps is the friendliest person I met on campus, who has helped me in a hundred different ways. I would also like to thank our group secretaries Donna Fackler, Jo Miller, and Joyce Lucas. Mohammed Mohammed has been a long-time philosopher friend and mentor to me. I would also like to thank the ECE academic advising office for helping me on many occasions. Thanks to Jan Progen, ECE publications office, for carefully reading this disseration.

I would not have survived graduate school, if not for friends outside work. Venkat, Karthik, Gayathri, Sreeram, Rajan, Anjan, Shankar, Anand, Vivek, Arvind, Ramsai, Jayanand, Jay, Siva theja, Hemant, Kunal, Vijay, and Fawad have made my stay at Champaign-Urbana memorable. Volleyball has helped me maintain sanity over the years, thanks to the different volleyball groups on campus with whom I played. Special thanks to Naghnaeian and Santiago for constantly pushing me to play better. My sister and her family have been a welcome distraction from work.

I thank my parents for their unselfish love, support and constant encouragement throughout my life. Finally I thank the eternal spirit which guides us all.

TABLE OF CONTENTS

LIST OF TABLES viii

LIST OF FIGURES ix

LIST OF ABBREVIATIONS xv

CHAPTER 1 INTRODUCTION 1

CHAPTER 2 MOLECULAR DYNAMICS STUDY OF DNA ELECTROPHORESIS THROUGH GRAPHENE NANOPORES 5
2.1 Introduction 5
2.2 Methods 6
2.3 Open nanopore resistance 10
2.4 Voltage-dependent kinetics of DNA transport through nanopore 13
2.5 Partially folded dsDNA transport 18
2.6 Influence of pore charge on DNA translocation 21
2.7 Detecting A-T and G-C base pairs with a graphene nanopore . 21
2.8 Conclusions 25

CHAPTER 3 GRAPHENE QUANTUM POINT CONTACT TRANSISTOR FOR DNA SENSING 28
3.1 Introduction 28
3.2 Structure description 29
3.3 Methods 30
3.4 Conductance variations due to external charges 33
3.5 Electrical response to DNA translocation 34
3.6 Conclusion 40

CHAPTER 4 ELECTRONIC DETECTION OF DSDNA TRANSITION FROM HELICAL TO ZIPPER CONFORMATION USING GRAPHENE NANOPORES 41
4.1 Introduction 41
4.2 Model and methods 42
4.3 Forced extension of dsDNA 45
4.4 DNA conformation detection using transverse electronic conductance 49

4.5 Conclusion 56

CHAPTER 5 DETECTING SSDNA TRANSLOCATION AT SINGLE BASE PAIR RESOLUTION 59
5.1 Introduction 59
5.2 Methods 59
5.3 Results and discussion 60
5.4 Conclusion 66

CHAPTER 6 SUMMARY 68

REFERENCES 69

LIST OF TABLES

2.1 List of performed simulations. 5
2.2 Breathing fluctuations of graphene around the pore from simulations SimA2, SimA7 and SimA8. 13
2.3 Details of voltage-dependent DNA translocation. This table complements Figure 2.4. The reduction in current is determined as 100−(Average blockade current/Open pore current)×100. 16

LIST OF FIGURES

2.1 Atomic model of the graphene nanopore system simulated in this study. Shown is dsDNA in its initial upright position inside a graphene nanopore of 2.4 nm diameter; also shown are K^+ and Cl^- ions, as well as the water surface at the boundaries of the simulated periodic cell (96 Å × 96 Å × 220 Å). 7

2.2 Open pore characteristics. (a) Graphene nanopore resistance. Circles represent the open pore resistance of a nanopore with diameter varying from 2 to 7 nm (SimA1-SimA6). The solid line is a $1/d^2$ fit to the circles (bias voltage is 3 V). The inset shows the I-V curve for a pore diameter of 3 nm. (b) Averaged potential map along the (x, z)-plane for a 2 nm diameter pore. (c) Same as in (b), but for a 7 nm diameter pore. The dashed line shows the potential change normal to the graphene membrane, illustrating the highly non-uniform potential profile. 11

2.3 Averaged potential maps along the (x, z)-plane for pore diameter (a) 2 nm, (b) 3 nm, (c) 4 nm, (d) 5 nm, (e) 6 nm and (f) 7 nm. The dashed line shows the potential change normal to the graphene membrane. 13

2.4 Electrophoresis of dsDNA through graphene nanopores. Shown is the ionic current (blue line) and position of DNA center of mass (black solid line) for bias voltages of (a) 4.3 (SimB1), (b) 2.5 (SimB2) and (c) 0.8 V (SimB3). The arrow indicates the time instance when DNA exits the pore. The black dashed line shows the average open pore current. Also shown is the averaged potential map in the (x, z)-plane for voltage biases of (d) 4.3, (e) 2.5 and (f) 0.8 V. A snapshot of DNA is shown at the right of each potential map (pore diameter is 2.4 nm). 15

2.5 Comparison of DNA center of mass (CoM) motions for various applied bias voltages. 17

2.6 Translocation of partially folded dsDNA (SimC). Shown is the time evolution of the ionic current. The three dotted lines correspond to plateaus in ionic current signature. Snapshots of DNA conformation during translocation is shown in (a) to (e): (a) initial conformation of dsDNA; (b) DNA captured by pore mouth; (c) both chains of folded DNA in the pore; (d) one chain leaves pore; (e) DNA exits the pore completely. The diameter of the pore is 3 nm and the bias voltage was 2.1 V. 19
2.7 Effect of pore charges on translocation. (a) Ionic current for p-charged (SimD1) and n-charged (SimD2) pores. (b) Displacement of the DNA center of mass for p- and n-charged pores. (c) Typical configuration of DNA in the p-charged pore. (d) Typical configuration of DNA in the n-charged pore. DNA in the n-charged pore adopts a more stretched conformation than in the p-charged pore. (The geometrical diameter of the pore is 2.4 nm, the bias voltage is 1 V and the total charge on the pore mouth is ± 3.6 e.) . . 20
2.8 Profiles of K^+ (red line) and Cl^- (blue line) ion currents for (a) an n-charged pore and (b) a p-charged pore. 22
2.9 Ionic current for poly(A-T)$_{20}$ and poly(G-C)$_{20}$ duplexes measured at 0.1 V, 0.3 V, 0.5 V, 1.0 V and 1.2 V transmembrane bias voltages in a 2.4 nm diameter nanopore (SimE1-SimF5). Translocation of A-T and G-C base pairs results in different ionic currents at 0.3 V, 0.5 V and 1.0 V. The snapshot shows that poly(A-T)$_{20}$ (red) is more stretched and disordered than poly(G-C)$_{20}$ (blue) at 1.0 V. The inset shows the number of base pairs near the pore mouth (±2 nm): A-T base pairs are more readily broken than G-C base pairs at 1.0 V. Figure 2.10 shows the number of base pairs near the pore mouth for 0.1 V, 0.3 V, 0.5 V and 1.2 V. 23
2.10 Number of base pairs near the pore mouth (±2 nm) for (a) 0.1 V, (b) 0.3 V, (c) 0.5 V and (d) 1.2 V. 24

3.1 Schematic diagram of a prototypical solid-state, multilayer device containing a GNR layer (black) with a nanopore, sandwiched between two oxides (transparent) atop a heavily doped Si back gate, V_G (green). The DNA is translocated through the pore, and the current is measured with the source and drain leads, V_S and V_D (gold). 30

3.2 Change in the conductance due to adding an external charge within the 2 nm pore. "S" means the charge is placed one half radius south of the center of the pore, and "W" means the charge is placed one half radius west of the center of the pore. (a) 5-GNR, (b) 15-GNR, (c) 8-QPC, and (d) 23-QPC. 35
3.3 (a) Schematic of an AT DNA strand translocating through a pore. (b) Potential maps in the graphene plane due to the DNA molecule at eight successive snapshots throughout one full rotation of the DNA strand. 36
3.4 Conductance as a function of DNA position (snapshot) for multiple Fermi energies, 0.04 eV (solid), 0.08 eV (long dash), 0.12 eV (short dash), and 0.16 eV (dot dash), as the DNA strand rigidly translocates through a 2.4 nm nanopore pore located at the device center (point P). (a) 5-GNR, (b) 15-GNR, (c) 8-QPC, and (d) 23-QPC. 38

4.1 Model of the simulated system. (a) All-atom MD model comprising of a 15-bp-dsDNA, K^+ and Cl^- ions, and water box. The dimensions of the simulated periodic cell were 70 Å×70 Å×110 Å. (b) Schematic of graphene nanopore system used to calculate the transverse electronic conductance. Shown in the figure is the snapshot of a DNA conformation that arose during one of the MD simulations. The DNA being extended was placed after the actual MD simulations inside a QPC edge nanopore to mimic an actual translocation process through the pore. The electrostatic potential surrounding the DNA was calculated and fed into a NEGF calculation of the transverse electronic conductance induced by the potential in the graphene membrane. A pore diameter of 2.4 nm was assumed. 43
4.2 Five representative snapshots (A-E) from a single SMD trajectory of poly(A-T)$_{15}$ DNA during a B-DNA (A) to zip-DNA (E) transition. The atoms colored in red were pulled in the z-direction at a rate of 1Å/ns; the blue colored atoms were harmonically restrained to the initial positions. Also shown is the evolution of two sets of base pairs, P-P' and Q-Q', which are a half pitch (namely 5 bp) apart. The black arrows, joining P to P' and Q to Q', initially pointing in opposite directions corresponding to a pure helical conformation (B-DNA) align themselves in the same direction once the zipper conformation (zip-DNA) is reached. The numbers below each snapshot represent the corresponding molecular extension. 46

4.3 Molecular extension of poly(A-T)$_{15}$ DNA over the course of a 60-ns SMD simulation performed at a constant pulling speed of 1 Å/ns. 48
4.4 Force-extension curves for poly(A-T)$_{15}$ DNA. Shown are the force-extension curves that resulted from five independent SMD simulations, Sim 1-5, performed at a pulling speed of 1 Å/ns. The force-extension curve begins with a region corresponding to the elastic extension of B-DNA followed by a B-DNA to zip-DNA transition plateau. In the region beyond the plateau the zip-DNA undergoes elastic extension, which is characterized by a sharp linear increase in force. The inset shows the zip-DNA conformation at the end of the transition plateau. 49
4.5 Evolution of the angle between base pairs P-P' and Q-Q' (see Figure 4.2) for five independent SMD simulations, Sim 1-5, performed on poly(A-T)$_{15}$ DNA; the angle changes from -180° to 0° as the DNA segment between P-P' and Q-Q' transitions from helical to zipper form. 50
4.6 Snapshots of the electrostatic potential profile of B-DNA in the graphene membrane at 1 M KCl concentration. The electrostatic potential profiles (a-i) correspond to translocation of the DNA segment, comprising of base pairs between P-P' and Q-Q', through the nanopore. The B-DNA, due to the helical DNA conformation, rotates by 180° in the plane of the graphene membrane. Along with the DNA rotation the electrical field also rotates inside the graphene nanopore, which induces oscillations in the transverse electronic conductance. 51
4.7 Snapshots of the electrostatic potential profile of zip-DNA in the graphene membrane at 1 M KCl concentration. The electrostatic potential profiles (a-i) correspond to translocation of the DNA segment, comprising of base pairs between P-P' and Q-Q', through the nanopore. The zip-DNA, due to the linear DNA conformation, does not rotate in the plane of the graphene membrane leading to a constant transverse electronic conductance. 52

4.8 Transverse electronic conductance as a function of poly(A-T)$_{15}$ DNA position (snapshot) for (a) graphene nanopore with armchair edge, and (b) graphene nanopore with QPC edge. base pairs P-P' were initially aligned with the nanopore, and subsequently translocated at a rate of 0.5 Å, along -z direction, per snapshot until base pairs Q-Q' reached the pore. The transverse electronic conductance changes from an oscillating type response, corresponding to B-DNA (A), to a constant conductance when the DNA adopts a zipper-like conformation, i.e., zip-DNA (E). Sinusoidal variation in the transverse electronic conductance diminishes as the DNA passes through the intermediate stages B,C, and D. A QPC edge geometry shows larger variations in transverse electronic conductance when compared to the armchair edge geometry. 53
4.9 The graphene lattices, with pore diameter = 2.4 nm, employed in the calculation of transverse electronic conductance: (a) 5 nm-wide armchair edge nanoribbon and (b) 8 nm-wide QPC edge nanoribbon. 54
4.10 Variation in the transverse electronic conductance as a function of DNA extension for a QPC edge graphene nanopore. Shown in (a) and (b) are conductance variation, for the stages A, B, C, D, and E (see Figure 4.2) arising in the B-DNA to zip-DNA transition corresponding to KCl molar concentrations of 1 M and 0.1 M respectively. The error bars are obtained from sampling over five independent force-extension simulations performed on poly(A-T)$_{15}$ and poly(G-C)$_{15}$ strands. 55
4.11 Snapshots of the electrostatic potential profile of B-DNA in the graphene membrane at 0.1 M KCl concentration. The electrostatic potential profiles (a-i) correspond to translocation of the DNA segment, comprising of base pairs between P-P' and Q-Q', through the nanopore. Due to reduced screening the electrostatic potential profile has a slower spatial decay when compared to the 1 M case (see Figure 4.6). 56
4.12 Radial distribution of electrostatic potential at the nanopore edge under KCl molar concentrations of 1 M and 0.1 M. The potentials correspond to a DNA conformation, where the base pair P-P' is inside the nanopore. At low molarity the potential in the vicinity of the pore is much larger (in magnitude) than 1 M case due to reduced screening. 57

5.1 Schematic of the graphene nanopore system used to calculate transverse electronic conductance. Shown in the figure is the ssDNA conformation, which arose from a MD simulation of forced extension of ssDNA. The extended ssDNA was placed inside a QPC edge graphene nanoribbon (g-QPC) and translocated at a rate of 1 Å per snapshot. Transverse electronic conductance was computed for the five base pairs shown in the inset of the figure. 61
5.2 Transverse electronic conductance, as a function of DNA position (snapshot), arising in a QPC-edged graphene membrane due to translocation of five base pairs of an ssDNA molecule in a linear ladder-like conformation (see inset Figure 5.1). The dips in the conductance correspond to the translocation of a single base pair through the nanopore. Three different nanopore geometries are investigated (a) nanopore center is aligned to the geometric center of the graphene membrane, (b) nanopore center is offset by 1 nm from the geometric center, and (c) nanopore center is offset by 2 nm from the geometric center. For each of the geometries the base pairs were translocated in two different configurations: (d) ssDNA-x, where the base pairs are aligned in the direction of transverse electronic current and (e) ssDNA-y where the base pairs are aligned in direction perpendicular to the transverse electronic currents. The coordinate axis is shown in (f). 63
5.3 Influence of pore size and shape on electronic conductance due to translocation of five base pair long ssDNA segment in a linear ladder-like conformation. Shown in the figure are conductance for the cases (a) circular pore with diameter = 1.2 nm, (b) circular pore with diameter = 2 nm, and (c) elliptical pore with major and minor axis diameters equal to 1.2 nm and 0.8 nm respectively. 65

LIST OF ABBREVIATIONS

MD	Molecular Dynamics
NEGF	Non-Equilibrium Green's Function
DNA	Deoxyribonucleic Acid
dsDNA	Double-Stranded DNA
ssDNA	Single-Stranded DNA
QPC	Quantum Point Contact
RMSD	Root Mean Square Deviation
FET	Field Effect Transistor
GNR	Graphene Nanoribbon

CHAPTER 1

INTRODUCTION

Nanopore based sequencing is a promising technology, to achieve low-cost and rapid DNA sequencing of the human genome, which can lead to a tremendous advancement in the field of personalized medicine [1]. A nanometre sized membrane, with a tiny pore, separates an ionic solution into two chambers. The DNA molecule is electrophoretically driven through the nanopore and the translocating molecule is probed electronically to decipher the passing nucleotides. The detection methods proposed are based on measuring ionic blockade currents [2], recording the electrostatic potential, induced by the DNA, using a nanopore capacitor [3], and using transverse currents to probe translocating DNA in a plane perpendicular to the translocation direction [4].

The driving electric field across the nanopore causes a steady ionic current to flow in the nanopore system. The charged biomolecule, driven electrophoretically by the field, translocates through the nanopore, transiently blocking the flow of ions causing blockade of ionic current. Different molecules block the pore to different characteristic degrees, resulting in ionic current blockade of different amplitude and duration. In the case of DNA, four nucleotides, namely A, T, G and C, in principle, yield distinct ionic current blockades. There has been a lot of effort to build DNA sequencing devices based on the expectation that a sequence-dependent blockade current can be resolved [1, 5].

Biological protein pores, e.g., α–hemolysin, were the first nanopores for which the possibility of building a sensor to sequence DNA was explored [2]. Experiments on α–hemolysin demonstrated reduction in current by an order of magnitude when a DNA molecule is present in the pore [2, 6]. Although having shown much promise, the high sensitivity of protein pores to temperature, pH and applied bias has been a major drawback for use in practical

applications [5].

Solid-state nanopores, fabricated in membrane materials like SiO_2 [7], Si_3N_4 [8], Al_2O_3 [9] and plastic [10], have emerged as an exciting alternative to protein pores as they are not only robust to the environment but also permit manipulation of physical and chemical properties of nanopores, in addition to bringing the advantage of being readily integrated into semiconductor devices and chips [5]. There has been extensive study on double-stranded DNA (dsDNA) translocation [8, 11, 12, 13, 14, 15, 16, 17, 18, 19, 20, 21, 22], single-stranded DNA (ssDNA) translocation [12, 23] and protein translocation [24, 25], through solid-state pores. A wealth of interesting results have been obtained with solid-state nanopores such as translocation time as a function of DNA length [11], salt-dependence on ion transport during DNA translocation [20, 21, 26], unzipping of DNA during translocation [15, 27] and discrimination of ssDNA and dsDNA based on pore diameter [12, 28]. However, solid-state nanopores are typically tens of nanometers thick, making it difficult to detect individual base-specific modulation in ion currents as multiple base pairs interact with the nanopore channel simultaneously [29].

Recently, proof of concept to realize and use graphene nanopores for DNA detection has been demonstrated experimentally [30, 31, 32]. Graphene is a material with extraordinary electrical and mechanical properties [33]. It is the thinnest known material with thickness equal to one atomic layer of carbon ~ 3 Å [34], which is comparable to the DNA base pair stacking distance of ~ 3.4 Å, making the graphene nanopore a promising device for DNA sequencing. The experiments have shown current blockades associated with translocation of dsDNA [30, 31, 32] and ssDNA [35]. In experiments, the DNA moved at velocities too high to permit resolution of individual base pair-specific current blockades. However, researchers have estimated theoretically that at slow translocation speeds a spatial resolution of 3.5 Å can be obtained with a 2.4 nm pore; this resolution equals the spacing between single base pairs in DNA [32].

Graphene, unlike biological and most solid-state membranes, is electrically active and can conduct electronic currents. Hence, another opportunity for sequencing DNA using graphene is based on transverse electronic currents

through the graphene membrane [36, 37, 38, 39, 40, 41]. Microampere sheet current conduction through graphene nanoribbons (GNR) with small pore diameters (2 nm) has been demonstrated experimentally [42]. Recent experiments have demonstrated further use of electronic sheet currents for the detection of DNA employing a graphene nanopore in the context of a graphene nanoribbon transistor [43].

Large scale molecular dynamics (MD) simulations, which resolve atomic level detail, have been used as a tool to study bionano systems [44, 45], and have been quite successful in investigating electric field-driven DNA translocation through α-hemolysin [6, 46] and Si_3N_4 [12, 13, 14, 47, 48] nanopores. Such simulations should also faithfully describe electric field-driven transport through graphene nanopores. Chapter 2 presents an atomic level description of DNA electrophoresis through graphene nanopores. Resolving at the atomic level electric field-driven DNA translocation is crucial to guide the design of graphene-based sequencing devices. Molecular dynamics simulations, in principle, can achieve such resolution and are employed here to investigate the effects of applied voltage, DNA conformation and sequence as well as pore charge on the translocation characteristics of DNA. We demonstrate that such simulations yield current characteristics consistent with recent measurements and suggest that under suitable bias conditions A-T and G-C base pairs can be discriminated using graphene nanopores.

In Chapter 3, we explore DNA detection using transverse electronic conductance in graphene membranes. Using Non-Equilibrium Green's Function (NEGF) technique, combined with a self-consistent Poisson-Boltzmann formalism to account for ion charge screening in the solution, we predict the possibility of detecting the rotational and positional conformation of a DNA strand inside the graphene nanopore. In particular, we show that a graphene membrane with Quantum Point Contact (QPC) geometry exhibits greater electrical sensitivity than a uniform armchair geometry provided that the carrier concentration is tuned to enhance charge detection. We propose a membrane design that contains an electrical gate in a configuration similar to a field effect transistor for a graphene-based DNA sensing device.

Mechanical manipulation of DNA, by forced extension, can lead to a struc-

tural transformation of double-stranded DNA (dsDNA) from a helical form to a linear zipper-like form. In Chapter 4 we show by employing molecular dynamics and NEGF-based transport simulations, the ability of graphene nanopores to discern different dsDNA conformations, in a helical to zipper transition, using transverse electronic conductance. In particular, conductance oscillations due to helical dsDNA vanish as dsDNA extends from helical to zipper form. The predicted ability to detect conformational changes in dsDNA, via transverse electronic conductance, can widen the potential of graphene-based nanosensors for DNA detection.

Finally in Chapter 5, we show that it is possible to discretely count individual base pairs of translocating ssDNA molecule through a graphene nanopore using transverse electronic conductance. Our study shows that the position of the pore can drastically enhance the shape of the conductance signals. Further, we show that the diameter and shape of the pore play a significant role in the sensitivity of calculated conductance signal.

CHAPTER 2

MOLECULAR DYNAMICS STUDY OF DNA ELECTROPHORESIS THROUGH GRAPHENE NANOPORES

2.1 Introduction

Table 2.1: List of performed simulations.

	Number of atoms	Temperature (K)	KCl conc. (M)	DNA (bp)	Diameter of pore (nm)	Pore charge (e)	Voltage (V)	Time (ns)
SimA1	126,277	295	1	–	2	0	3.0	7
SimA2	126,308	295	1	–	3	0	3.0	7
SimA3	126,355	295	1	–	4	0	3.0	7
SimA4	126,435	295	1	–	5	0	3.0	7
SimA5	126,540	295	1	–	6	0	3.0	7
SimA6	126,653	295	1	–	7	0	3.0	7
SimA7	126,308	295	2	–	3	0	3.0	7
SimA8	126,308	305	1	–	3	0	3.0	7
SimB1	188,743	295	1	45	2.4	0	4.3	3
SimB2	188,743	295	1	45	2.4	0	2.5	5
SimB3	188,743	295	1	45	2.4	0	0.8	35
SimB4	188,743	295	1	45	2.4	0	0.1	50
SimC	217,053	295	1	55	3	0	2.1	14.5
SimD1	210,670	295	1	45	2.4	+3.6	1.0	23
SimD2	210,670	295	1	45	2.4	-3.6	1.0	28
SimE1	210,772	295	1	poly(A-T)$_{45}$	2.4	0	0.1	20
SimE2	210,772	295	1	poly(A-T)$_{45}$	2.4	0	0.3	20
SimE3	210,772	295	1	poly(A-T)$_{45}$	2.4	0	0.5	20
SimE4	210,772	295	1	poly(A-T)$_{45}$	2.4	0	1.0	10
SimE5	210,772	295	1	poly(A-T)$_{45}$	2.4	0	1.2	10
SimF1	210,772	295	1	poly(G-C)$_{45}$	2.4	0	0.1	20
SimF2	210,772	295	1	poly(G-C)$_{45}$	2.4	0	0.3	20
SimF3	210,772	295	1	poly(G-C)$_{45}$	2.4	0	0.5	20
SimF4	210,772	295	1	poly(G-C)$_{45}$	2.4	0	1.0	10
SimF5	210,772	295	1	poly(G-C)$_{45}$	2.4	0	1.2	10

All-atom molecular dynamics (MD) simulations can investigate microscopic kinetics of DNA translocation through graphene nanopores at atomic-scale resolution. We performed the series of all-atom MD simulations listed in

Table 2.1, covering altogether 370 ns, to provide an atomic level description of DNA translocation through graphene nanopores as shown in Figure 2.1. The simulations characterize the influence of several key factors on ionic current signals expected to resolve DNA sequence, namely, pore size, strength of an external electric field, DNA conformation, and pore charge. The simulations suggest that A-T and G-C base patterns can be resolved. In our study, first the relationship between the resistance of a graphene nanopore and its size was determined through monitoring I-V curves in open pore MD simulations. Second, the effects of applied voltage bias on the kinetics of DNA translocation through a nanopore were investigated. Third, we simulated the translocation of partially folded double-stranded DNA to determine the effect of DNA conformation on current signals. Fourth, the influence of pore charge on DNA translocation was studied. Finally, we computed the blockage current caused by poly(A-T)$_{20}$ and poly(G-C)$_{20}$ duplexes to explore the feasibility of base pair resolution in graphene nanopores.

2.2 Methods

2.2.1 Molecular dynamics simulations

In MD simulations, atoms are treated as point particles with intrinsic properties such as charge, radius, mass, etc., which affect their interactions with the surrounding atoms during simulations. Interactions among atoms are governed by the potential energy of the system, which is described by Eq. 2.1. The first three terms describe "bonded interaction," which arise from bonds, angles and dihedrals in covalent bonded systems. The last two terms describe the "non-bonded" interactions which include van der Waals interaction, represented by Lennard-Jones potentials and an expression for Coulomb

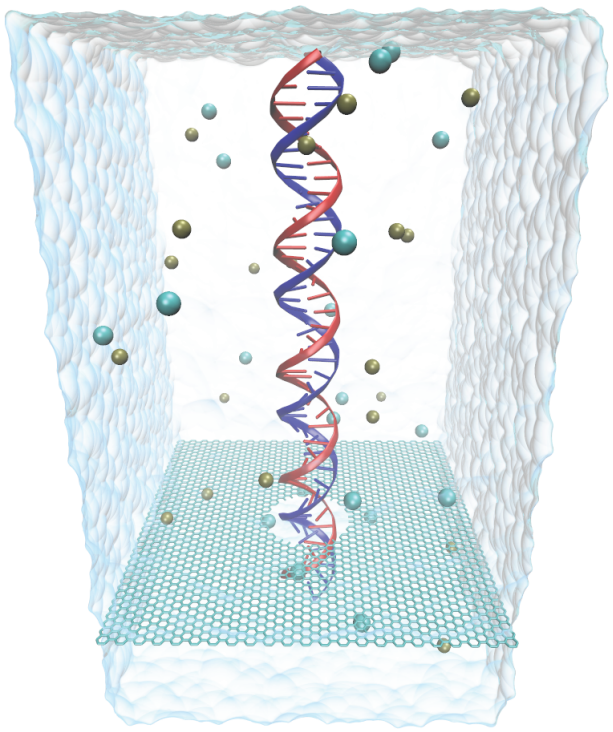

Figure 2.1: Atomic model of the graphene nanopore system simulated in this study. Shown is dsDNA in its initial upright position inside a graphene nanopore of 2.4 nm diameter; also shown are K^+ and Cl^- ions, as well as the water surface at the boundaries of the simulated periodic cell (96 Å × 96 Å × 220 Å).

interaction.

$$U_{MD}(\vec{R}) = \sum_{bond} k_i^{bond}(r_i - r_0)^2 + \sum_{angles} k_i^{angle}(\theta_i - \theta_0)^2 + \sum_{dihedrals} k_i^{dihedral}[1 + cos(n_i\phi_i + \delta_i)] + \sum_i \sum_{j>i} 4\epsilon_{ij}\left[(\frac{\sigma_{ij}}{r_{ij}})^{12} - (\frac{\sigma_{ij}}{r_{ij}})^6\right] + \sum_i \sum_{j>i} \frac{q_i q_j}{4\pi\epsilon_0 r_{ij}} \quad (2.1)$$

The forces acting on atoms are evaluated using the above potential energy function. The trajectories of all atoms can be traced, given the initial position and velocities, by evolving the atoms according to Newton's second law [49].

2.2.2 System setup

The lattice points $\vec{r}_{\rm mn}$ for the graphene membrane used in the simulations, $\vec{r}_{\rm mn}$ = m $\vec{a}_1$ + n $\vec{a}_2$, m, n $\in$ $\mathbb{Z}$, were constructed using 2D lattice vectors $\vec{a}_1 = \left(\frac{\sqrt{3}}{2}a, \frac{a}{2}\right)$ and $\vec{a}_2 = \left(\frac{\sqrt{3}}{2}a, -\frac{a}{2}\right)$, where $a = \sqrt{3} \times a_{\rm C-C} = 2.46$ Å and $a_{\rm C-C}$ is the distance between two carbon atoms, namely, 1.42 Å. Each unit cell for graphene has two atoms, one at $\vec{r}_{\rm mn}$ and one at $\vec{r}_{\rm mn}$ + (a, 0). The pore is constructed by removing atoms whose coordinates satisfy the condition $x^2 + y^2 \leq d^2$, where d is the diameter of the pore. Periodic boundary conditions are applied at the boundary of the perforated graphene membrane simulated.

A double-stranded helix of DNA was built with the program X3DNA [50]. The topology of DNA along with the missing hydrogen atoms were generated using psfgen [49], with the resulting topology files corresponding to the CHARMM27 force field [51]. The system comprising DNA and graphene was solvated in a water box. Ions (1 M KCl) were randomly placed in the water box in a stoichiometry that achieved charge neutrality in the final system. The simulation details are listed in Table 2.1. Simulations SimD1 − SimF5 were done with 1/3 of the DNA inserted into the pore allowing translocation events to be observed within affordable computer time, i.e., the simulations avoided the time-consuming search of the DNA for pore entry. In simulations SimD1 and SimD2 each carbon atom on the pore mouth had a charge

of ± 0.1 e. The value of 0.1 e is based on previous calculations on carbon nanotubes, the ends of which were terminated with H atoms; in this case the partial charges on C atoms are ≈ -0.1 e [52].

All MD simulations were performed using the program NAMD 2.7 [49] employing periodic boundary conditions. CHARMM27 force field parameters were used for DNA [51], TIP3P water molecules [53] and ions. The parameters for carbon atoms of graphene were those of type CA in the CHARMM27 force field [51], namely the type of benzene carbons. The integration time step used was 1 fs with particle-mesh Ewald (PME) full electrostatics with grid density of $1/\text{Å}^3$. Van der Waals energies were calculated using a 12 Å cutoff. A Langevin thermostat was assumed to maintain constant temperature at 295 K [54].

The system was first minimized for 4000 steps, then heated to 295 K in 4 ps. After heating, 500 ps-equilibration with the DNA constrained was conducted under NPT ensemble conditions, using the Nosé-Hoover Langevin piston pressure control at 1 bar [54]. To prevent drift of the graphene membrane, carbon atoms at the boundary were restrained using harmonic forces with spring constant of 1 kcal mol^{-1} Å^{-2}. After the system acquired a constant volume in the NPT ensemble, 1.5 ns-equilibration was conducted in an NVT ensemble, constraining the end of DNA nearest to the pore. Finally, simulations were carried out as listed in Table 2.1 by applying a uniform electric field, directed normal to the graphene membrane, to all atomic partial charges in the system. The corresponding applied potential is $V_0 = -EL_Z$, where L_Z is the length of the simulation cell in the z-direction. The atoms rearrange themselves to produce an actual potential V (the sum of the potential from all simulated charges plus the applied voltage) with a profile that is non-uniform across the graphene membrane (see, for example, Figure 2.2).

2.2.3 Data analysis

In electronic measurements one can observe temporary drops in the measured conductance, arising from translocating DNA molecules partially blocking the pore [30, 31, 32]. Therefore, magnitude and duration of the ionic blockade

current reflect the properties of the DNA inside the pore. To characterize the ionic current under different DNA translocation conditions, we monitored the time-dependent ionic current $I(t)$ in MD simulations. The total ionic current $I(t)$ was computed as [47]

$$I(t) = \frac{1}{\Delta t L_z} \sum_{i=1}^{N} q_i \big[z_i(t + \Delta t) - z_i(t) \big] \tag{2.2}$$

where the sum runs over all ions, Δt was chosen to be 50 ps and z_i and q_i are the z coordinate and charge of ion i, respectively. L_z represents the system dimension in the z-direction.

To illustrate the influence of external voltage on the kinetics of DNA electrophoresis, potential maps were computed. The potential $V(\vec{r})$ due to DNA and ions in the system was computed by averaging the instantaneous electrostatic potential (corresponding to single trajectory frames) over the entire MD trajectory on a three-dimensional grid representing positions $\vec{r}$. The applied linear potential is then added at each grid point to give the final potential. The procedure is described in detail in [46]. The snapshots of the molecular structure from the MD simulations were depicted with VMD [55].

2.3 Open nanopore resistance

The ability of MD simulations to faithfully reproduce electric field-driven transport of ions through nanopores is crucial in describing DNA translocation-induced blockades in ionic current, presumably the signatures for DNA sequences, motivating the study of open pore characteristics of graphene membranes.

In order to assess the accuracy of MD simulations in describing ionic conductance of graphene nanopores, we compare the characteristics of nanopore resistance obtained from simulations with experiment. For this purpose, a series of all-atom MD simulations were carried out for the ionic current through open pores (for 1 M KCl) with pore diameters in the range 2-7 nm (see simulations SimA1-SimA6 in Table 2.1). Anions and cations are driven in opposite directions by an external electric field, resulting in a net current.

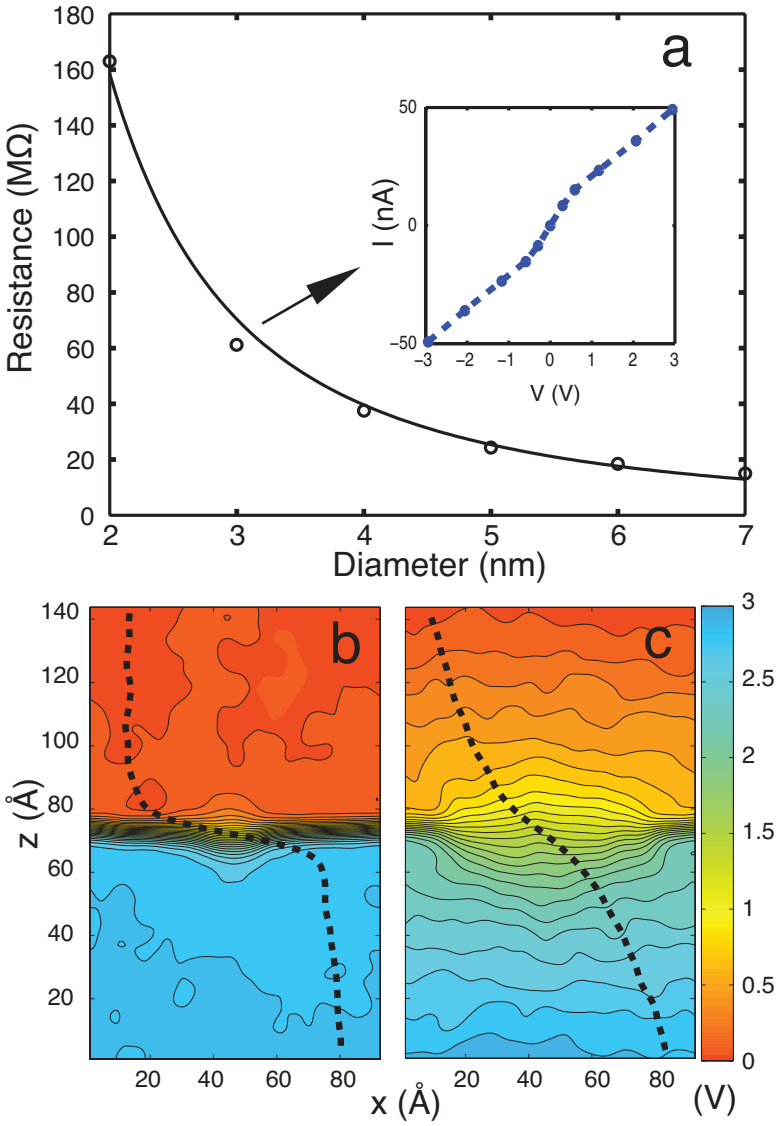

Figure 2.2: Open pore characteristics. (a) Graphene nanopore resistance. Circles represent the open pore resistance of a nanopore with diameter varying from 2 to 7 nm (SimA1-SimA6). The solid line is a $1/d^2$ fit to the circles (bias voltage is 3 V). The inset shows the I-V curve for a pore diameter of 3 nm. (b) Averaged potential map along the (x, z)-plane for a 2 nm diameter pore. (c) Same as in (b), but for a 7 nm diameter pore. The dashed line shows the potential change normal to the graphene membrane, illustrating the highly non-uniform potential profile.

Figure 2.2 shows the open pore resistance as a function of pore diameter d. The resistance is determined as $\langle I \rangle / V$ where $\langle I \rangle$ is the average ionic current through the pore during a 7 ns MD simulation. The dependence of resistance on the pore diameter follows closely the relationship $R \sim 1/d^2$, which agrees qualitatively with experiment [30]. The resistance values obtained through simulation are 3-4 times smaller than corresponding values in experiments. The discrepancy is attributed to: (i) higher voltage (3 V) used in simulations compared to experiments (0.1 V); (ii) the charge distribution and exact shapes of the graphene pores not being experimentally known; and (iii) inaccuracy of the force field assumed in the simulations that describes graphene-ion-water interactions poorly. The inset in Figure 2.2 shows a typical current-voltage (I-V) curve for a 3 nm-diameter pore at bias voltage of 3 V. The I-V curve is linear for low applied bias voltages. The motion of ions in the capture cross section of the pore is diffusion limited; hence, the linear I-V relationship breaks down at high fields [47].

To understand the size-dependence of pore resistance, the mean electrostatic potential in the system was calculated. Figures 2.2b, c show the averaged electrostatic potential maps in the (x, z)-plane for pore diameters of 2 and 7 nm, respectively. The potential maps for 3, 4, 5 and 6 nm diameter pores are provided in Figure 2.3. The potential maps illustrate that most of the potential drop arises across the membrane, not in the bulk. The potential drop becomes sharper near the membrane as the size of the pore decreases.

Simulations also revealed significant graphene membrane fluctuation. The magnitude of the fluctuation, reflecting a "breathing" of the nanopore, can be as large as the nanopore thickness (see Table 2.2). The breathing limits the spatial resolution of the ultra-thin graphene membrane to a value above its physical membrane thickness. Furthermore, the simulations show that increasing KCl concentration (SimA7) enlarges the fluctuation due to the increased number of voltage-driven ions colliding with the graphene membrane; an increase in temperature (SimA8) also leads to larger breathing fluctuation amplitudes (see Table 2.2).

Table 2.2: Breathing fluctuations of graphene around the pore from simulations SimA2, SimA7 and SimA8.

Pore Diameter (nm)	KCl Concentration (M)	Temperature (K)	Average RMSD fluctuation of pore mouth (Å)	Maximum RMSD fluctuation of pore mouth (Å)
3	1	295	0.72	3.3
3	2	295	0.93	4.4
3	1	305	1.7	4.4

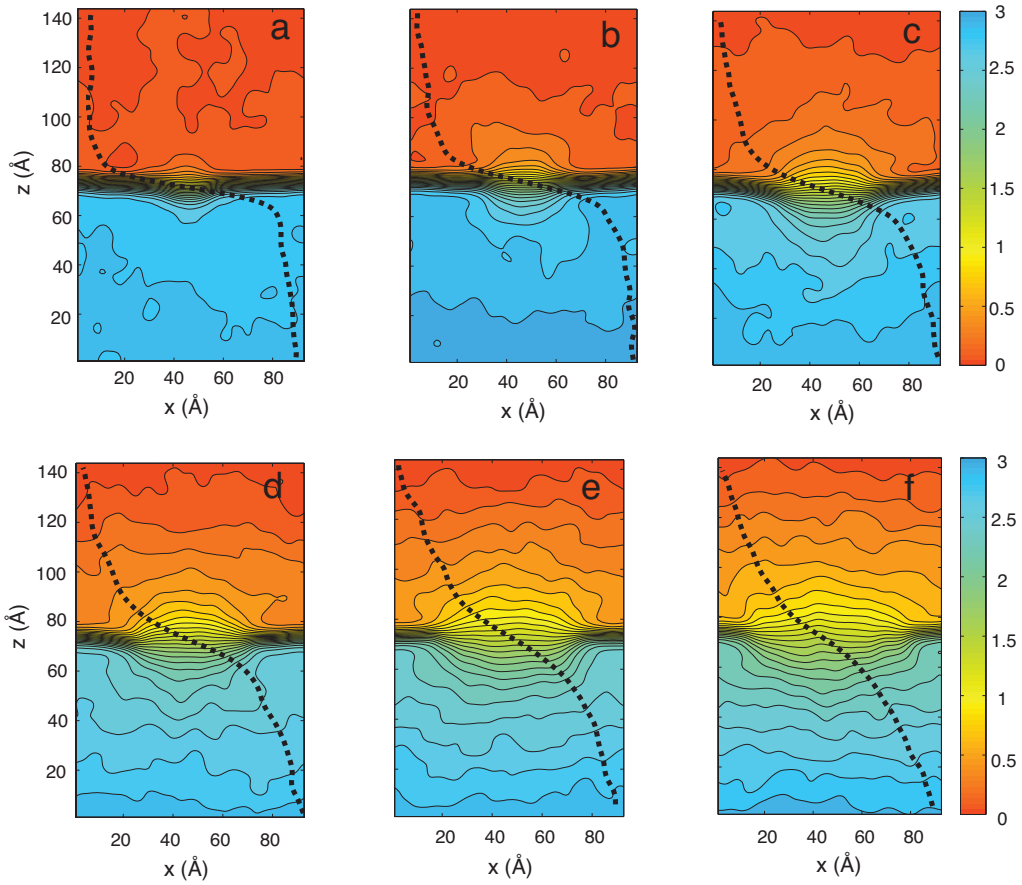

Figure 2.3: Averaged potential maps along the (x, z)-plane for pore diameter (a) 2 nm, (b) 3 nm, (c) 4 nm, (d) 5 nm, (e) 6 nm and (f) 7 nm. The dashed line shows the potential change normal to the graphene membrane.

2.4 Voltage-dependent kinetics of DNA transport through nanopore

We studied the electrophoresis of dsDNA (45 bp) through a 2.4 nm diameter graphene nanopore at bias voltages of 4.3, 2.5 and 0.8 V (for 1M KCl). The

pores used in experiments had diameters in the range 5-22 nm [30, 31]. In order to observe translocation events on computationally affordable simulation timescales, the minimum applied voltage bias, which had to be assumed in simulations, was 4-8 times larger than the voltage bias applied in experiments [30, 31]. In the simulations, DNA was placed initially in a linear head-tail configuration at the pore mouth (see Figure 2.1). The capture of DNA by the nanopore requires DNA to reach the pore by diffusion from the bulk and thread itself into the pore by crossing an entropic barrier [56, 57, 58]. For small pores the main potential drop arises in the pore (see Figure 2.2b) and, therefore, DNA can be captured in this case only after it has diffused close to the pore mouth. Simulation of the capture process itself would require long simulation times. Since we are interested in the kinetics of the actual DNA translocation through the pore, not in the capture of DNA, we placed the DNA in all simulations at the pore mouth.

Figures 2.4a-c show, for different bias voltages (4.3, 2.5 and 0.8 V), the time evolution of ionic current and displacement of the DNA center of mass (CoM) when DNA translocates through the graphene nanopore. The potential maps along with typical DNA conformation are also shown in Figures 2.4d-f. A characteristic blockade of the ion current occurs when DNA resides in the nanopore; when it exits the pore, the current returns back to the open pore value. For 0.8 V, the reduction in pore current during blockade is 56%, for 2.5 V it is 34% and for 4.3 V it is 12% (more detail is provided in Table 2.3). Apparently, DNA blocks the current more effectively at lower bias voltage. At high bias voltage (4.3 V), DNA is stretched to a larger extent compared to low bias voltage, 0.8 V, as shown in Figure 2.4d, allowing more ions to pass through the pore and resulting in less blockage of the current. The stretching of DNA at high bias voltages also explains the occasional overshoot of the blockade current above the open pore value. A spike in ion current is observed when the DNA leaves the pore and is due to rushing of clouds of K^+ and Cl^- ions (which accumulate near the pore mouth due to blockade by the DNA) through the empty pore once the DNA exits [47]; the overshoot is more prominent at higher bias voltages.

The translocation time for the DNA through the nanopore is 1.6, 3.7 and 27 ns for bias voltages of 4.3, 2.5 and 0.8 V, respectively. When a high

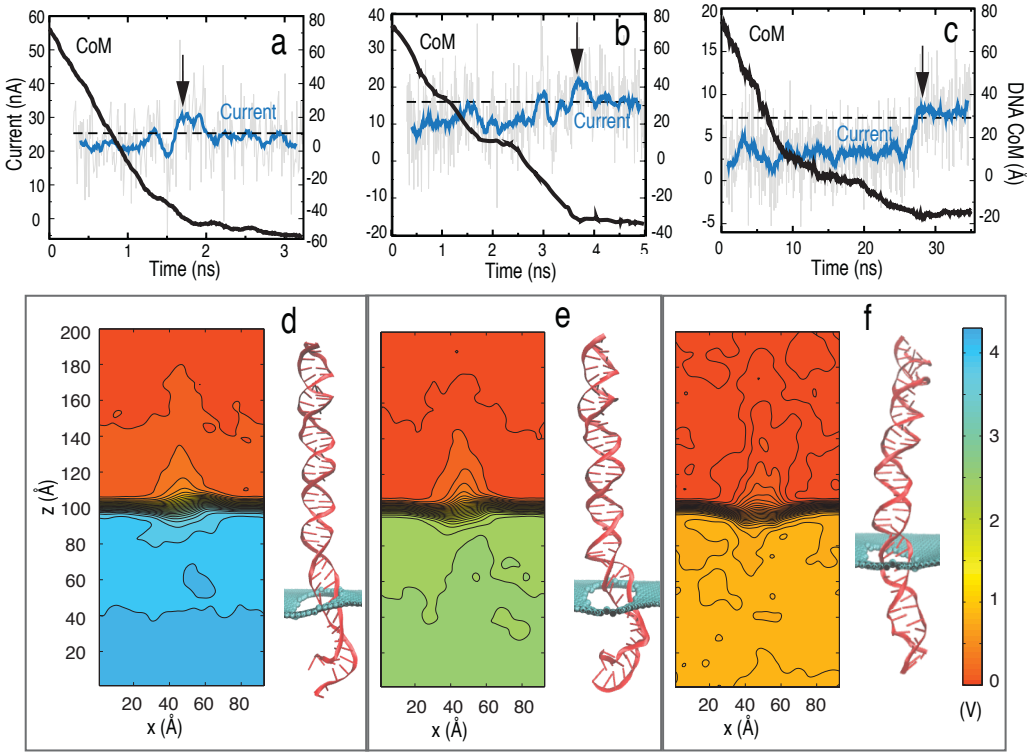

Figure 2.4: Electrophoresis of dsDNA through graphene nanopores. Shown is the ionic current (blue line) and position of DNA center of mass (black solid line) for bias voltages of (a) 4.3 (SimB1), (b) 2.5 (SimB2) and (c) 0.8 V (SimB3). The arrow indicates the time instance when DNA exits the pore. The black dashed line shows the average open pore current. Also shown is the averaged potential map in the (x, z)-plane for voltage biases of (d) 4.3, (e) 2.5 and (f) 0.8 V. A snapshot of DNA is shown at the right of each potential map (pore diameter is 2.4 nm).

bias voltage (4.3 V) is applied across the pore, DNA near the pore mouth adopts a stretched structure throughout the translocation period. The electric field is much stronger than the attractive hydrophobic force between DNA and graphene, which keeps the DNA in a vertical conformation as it moves through the pore, preventing the DNA to stick to the graphene membrane. Some of the DNA base pairs also unzip due to the high field. The DNA CoM moves at a constant velocity as indicated by the constant slope of the DNA CoM (during the translocation period) seen in Figure 2.4a. In the low bias voltage case (0.8 V) the DNA initially moves in the pore keeping its vertical conformation and remaining unstretched, but at around 10 ns the DNA starts to stick to the graphene membrane due to strong hydrophobic interaction and slows down its CoM movement, as shown in Figure 2.4c. The adhesion of translocated base pairs to the graphene membrane causes DNA in the pore to be stretched to a larger extent and partially unzip. At 2.5 V applied bias voltage the DNA slowed down briefly at 2.2 ns due to hydrophobic interaction between a base pair and the graphene membrane, but the hydrophobic interaction was not strong enough compared to the applied field and, hence, did not decrease the translocation speed of DNA as indicated by the slope of the displacement of the DNA CoM in Figure 2.4b. The translocation time depends inversely on the applied voltage in the absence of DNA interacting with the membrane [16, 59, 60]. However, the translocation rate of DNA through narrow pores is strongly affected by the interaction between DNA and nanopore surface [19]; the DNA translocation can even stall due to the interaction with graphene. The two slopes in the CoM time dependence seen in Figure 2.4c derive their distinctness from the role that the hydrophobic interaction plays during DNA translocation.

Table 2.3: Details of voltage-dependent DNA translocation. This table complements Figure 2.4. The reduction in current is determined as 100−(Average blockade current/Open pore current)×100.

Applied bias voltage (V)	Open pore current (nA)	Average blockade current (nA)	Reduction in current (%)	Translocation time (ns)
0.8	7.2	3.20	56	27.0
2.5	16.0	10.56	34	3.7
4.3	25.4	22.30	12	1.6

Finally, DNA translocation at a low bias voltage of 0.1 V (i.e., the bias voltage used typically in experiments) was simulated (SimB4), which resulted in three base pairs translocating through the graphene nanopore during 50 ns. Based on the corresponding translocation time of 17 ns/bp, the translocation time for a 45 bp DNA would be 0.75 μs at 0.1 V. This estimated time (0.75 μs), however, does not entirely take into consideration hydrophobic interactions of DNA with graphene, as the DNA in the 0.1 V simulation is just entering the pore mouth and does not yet establish strong hydrophobic interactions with the graphene membrane. The hydrophobic interactions are likely to increase the translocation time further. Figure 2.5 shows the DNA CoM as a function of time for various bias voltages. In DNA sequencing applications the DNA can be held in a stretched conformation to prevent translocation stalling and DNA sticking to the graphene membranes.

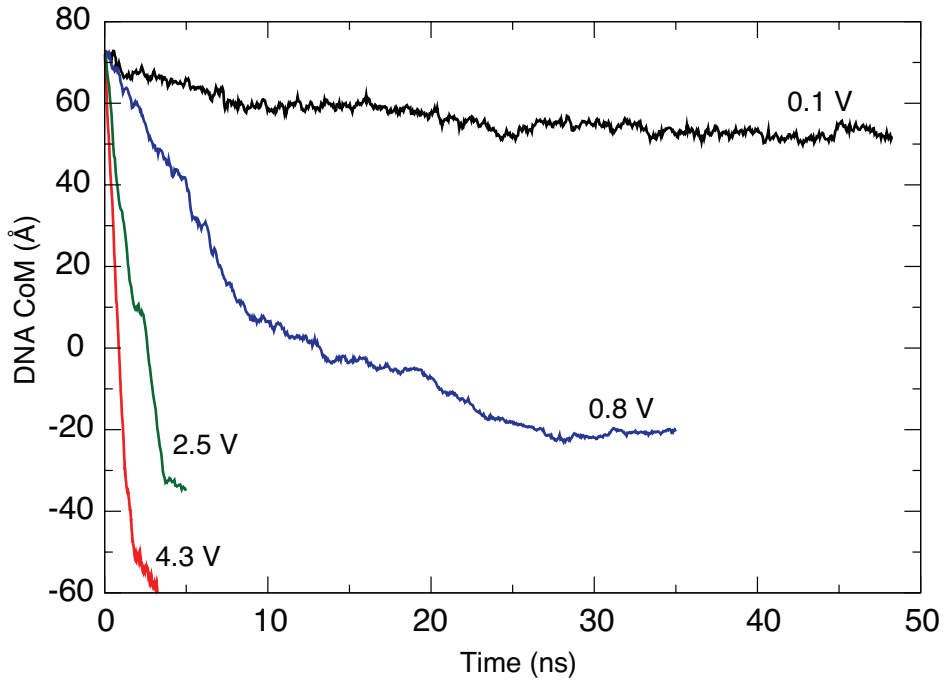

Figure 2.5: Comparison of DNA center of mass (CoM) motions for various applied bias voltages.

2.5 Partially folded dsDNA transport

DNA is a flexible polymer chain that adopts many different conformations in solution. When the length of DNA exceeds its persistent length, DNA may permeate through large pores ($d > 2$ nm) in a folded conformation, rather than in a linear head-to-tail fashion (unfolded). In electronic measurements of DNA translocation through nanopores, different current signatures have been observed [30, 31, 32], which were attributed to different types of translocation events. Translocation of folded DNA, which occupies at least twice the volume of unfolded DNA, resulted in stronger current blockades compared to unfolded DNA [11, 59, 61].

To provide an atomic level description of the translocation dynamics of partially folded DNA, we performed an MD simulation driving a 55-bp partially folded dsDNA through a 3 nm diameter nanopore (SimC). In the simulation, shown in Figure 2.6a-e, DNA was placed on top of the nanopore and close to the pore mouth. To ensure that DNA translocation happens on a time scale accessible for MD, a bias voltage of 2.1 V was applied. Under a high electric field, the partially folded DNA permeated the nanopore in 15 ns. Figure 2.6 demonstrates that partially folded dsDNA translocation results in two different current blockades: (i) when DNA is captured by the electric field (Figure 2.6a), the folded part is stretched such that two dsDNA chains are in the pore simultaneously (Figure 2.6b); the folded part of DNA blocks the pore resulting in an average current of $\sim$ 11 nA (Figure 2.6c). (ii) Once the folded part permeates through the pore, leaving only one dsDNA chain in the pore (Figure 2.6d), the average current increases to $\sim$19 nA. When the entire dsDNA exits the pore, the current reaches an average value of $\sim$ 26 nA (Figure 2.6e). The simulation reveals a characteristic double plateau current signature for translocation of partially folded dsDNA, which agrees well with experimental observation [30]. The folded dsDNA adopts a stretched conformation in order to squeeze through the pore as the latter is geometrically narrower ($d = 3$ nm) than the folded dsDNA (which has a diameter $d > 4$ nm).

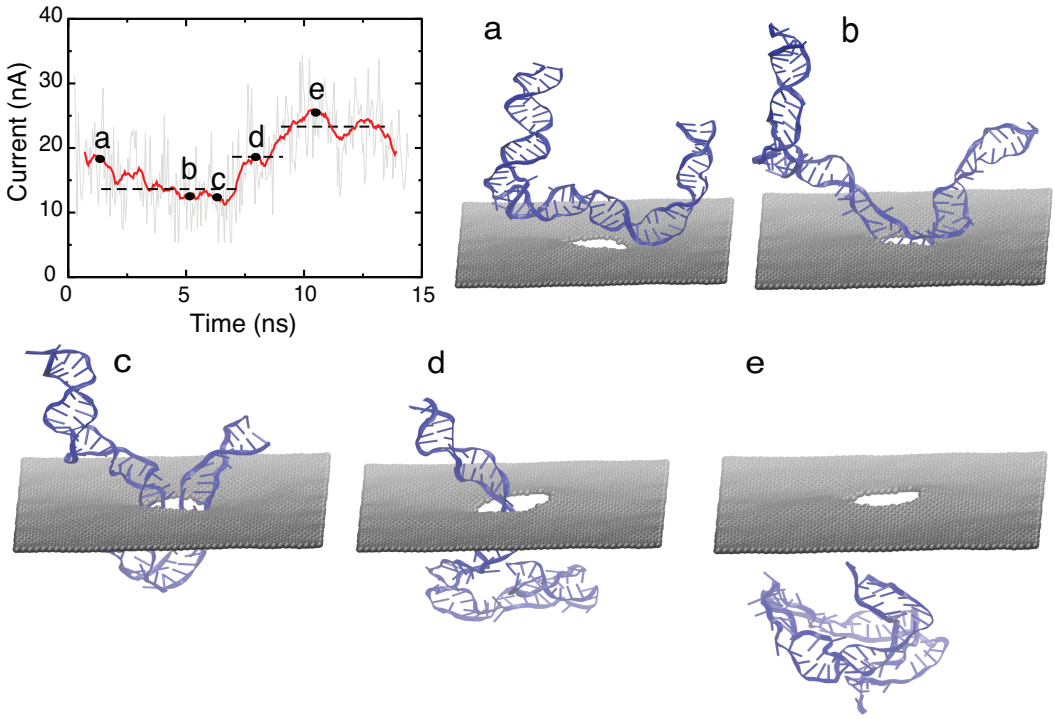

Figure 2.6: Translocation of partially folded dsDNA (SimC). Shown is the time evolution of the ionic current. The three dotted lines correspond to plateaus in ionic current signature. Snapshots of DNA conformation during translocation is shown in (a) to (e): (a) initial conformation of dsDNA; (b) DNA captured by pore mouth; (c) both chains of folded DNA in the pore; (d) one chain leaves pore; (e) DNA exits the pore completely. The diameter of the pore is 3 nm and the bias voltage was 2.1 V.

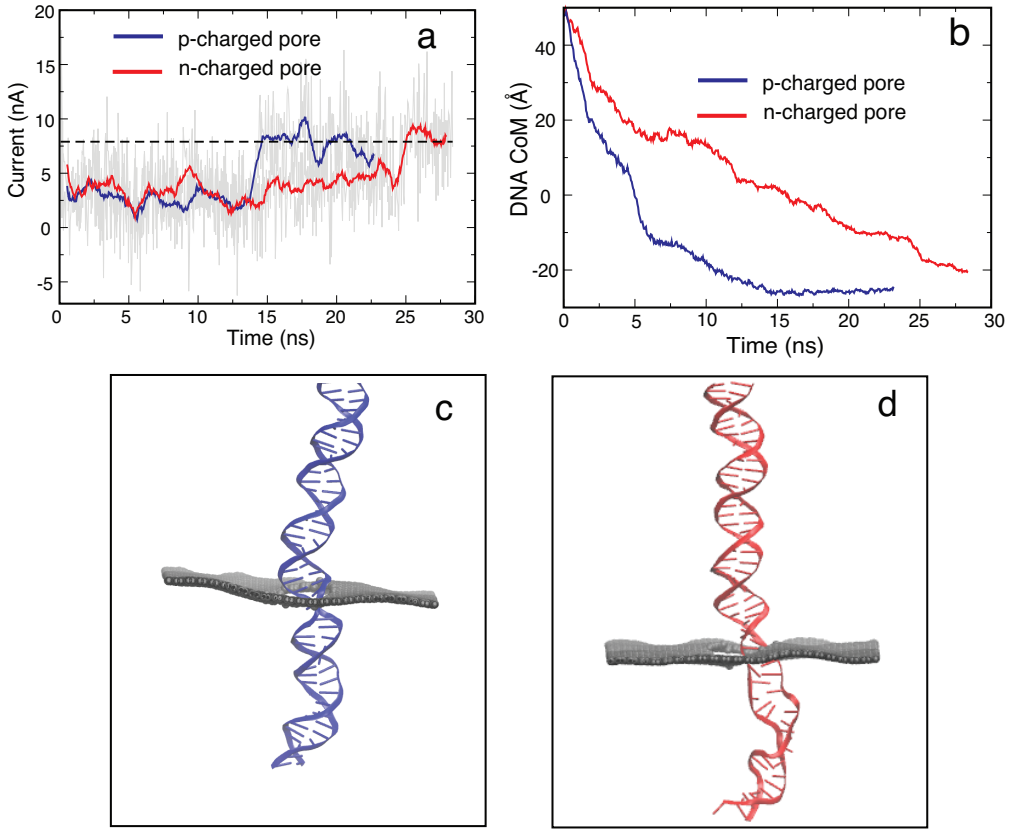

Figure 2.7: Effect of pore charges on translocation. (a) Ionic current for p-charged (SimD1) and n-charged (SimD2) pores. (b) Displacement of the DNA center of mass for p- and n-charged pores. (c) Typical configuration of DNA in the p-charged pore. (d) Typical configuration of DNA in the n-charged pore. DNA in the n-charged pore adopts a more stretched conformation than in the p-charged pore. (The geometrical diameter of the pore is 2.4 nm, the bias voltage is 1 V and the total charge on the pore mouth is $\pm$ 3.6 e.)

2.6 Influence of pore charge on DNA translocation

To determine the principle influence of pore charge on translocation kinetics of DNA, two pores with total charges ± 3.6 e were constructed, where each carbon atom on the pore mouth had a charge of ± 0.1 e. MD simulations on these two systems with bias voltage of 1 V were performed (SimD1 and SimD2). As shown in Figure 2.7a the translocation time for a negatively charged (n-charged) pore is 25 ns, while the translocation time for a positively charged (p-charged) pore is 15 ns. Figure 2.7b shows that DNA moves faster through a p-charged pore than through an n-charged pore. Since DNA is highly negatively charged itself, a repulsive interaction arises between a negatively charged pore and DNA which shrinks the diameter of the pore effectively. Figures 2.7c, d show that DNA adopts a conformation that is more stretched in the case of the n-charged pore than in the case of the p-charged pore. The stretched DNA blocks the pore to a smaller degree allowing more K^+ ions to pass through the pore along with DNA, but opposite to it (see Figure 2.8), leading to a higher hydrodynamic drag and, thus, slowing down the DNA in the n-charged pore. Previous studies on solid-state nanopores also revealed a similar trend [62]. The above simulations suggest that pore charge can slow down DNA translocation.

2.7 Detecting A-T and G-C base pairs with a graphene nanopore

Rapid DNA sequencing is a major goal of nanopore research. Previous studies pursued the goal to identify the four DNA bases (A, T, G, C) through analyzing current signals produced by DNA as it permeates through the nanopore [16, 61, 63, 64, 65, 66]. However, solid-state and biological nanopores have a pore thickness of > 5 nm [5, 21, 59, 67], which implies that multiple base pairs are inside the nanopore simultaneously. Hence, reducing the thickness of the nanopore is crucial for high-resolution DNA sequencing. Here, we demonstrate that A-T and G-C base pairs can be discriminated in dsDNA using an ultra-thin nanopore, namely a graphene nanopore with a physical membrane thickness of about 0.3 nm [34].

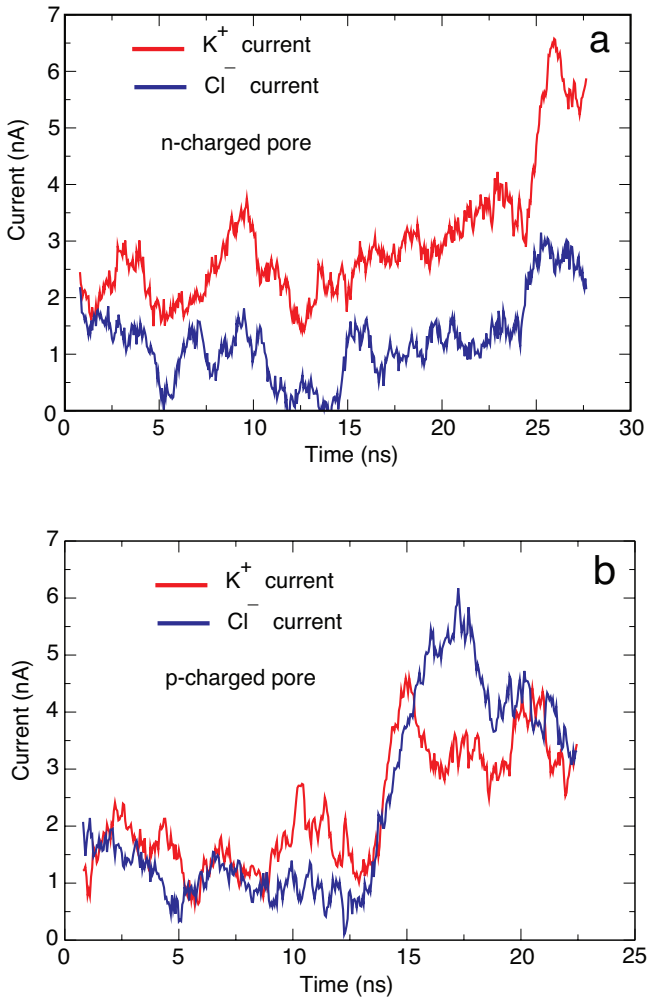

Figure 2.8: Profiles of K^+ (red line) and Cl^- (blue line) ion currents for (a) an n-charged pore and (b) a p-charged pore.

In MD simulations, poly(A-T)$_{20}$ and poly(G-C)$_{20}$ were inserted into a 2.4 nm pore and subjected to different bias voltages (0.1 V, 0.3 V, 0.5 V, 1.0 V and 1.2 V). To avoid DNA attaching to the graphene membrane, the two ends of DNA were subject to constraints, which allowed DNA to move freely only along the z-axis. Figure 2.9 demonstrates that at 0.1 V (lowest) and 1.2 V (highest) biases, the mean values of pore current of poly(A-T)$_{20}$ and poly(G-C)$_{20}$ are almost the same, while at intermediate bias values of 0.3 V, 0.5 V and 1.0 V the mean pore current of poly(A-T)$_{20}$ is larger than that of poly(G-C)$_{20}$. At 0.1 V, neither poly(A-T)$_{20}$ nor poly(G-C)$_{20}$ is stretched; hence, they block the nanopore to the same degree resulting in a pore current of $\sim$ 0.2 nA. At 0.3 V and 0.5 V, stretched by electric field, the base

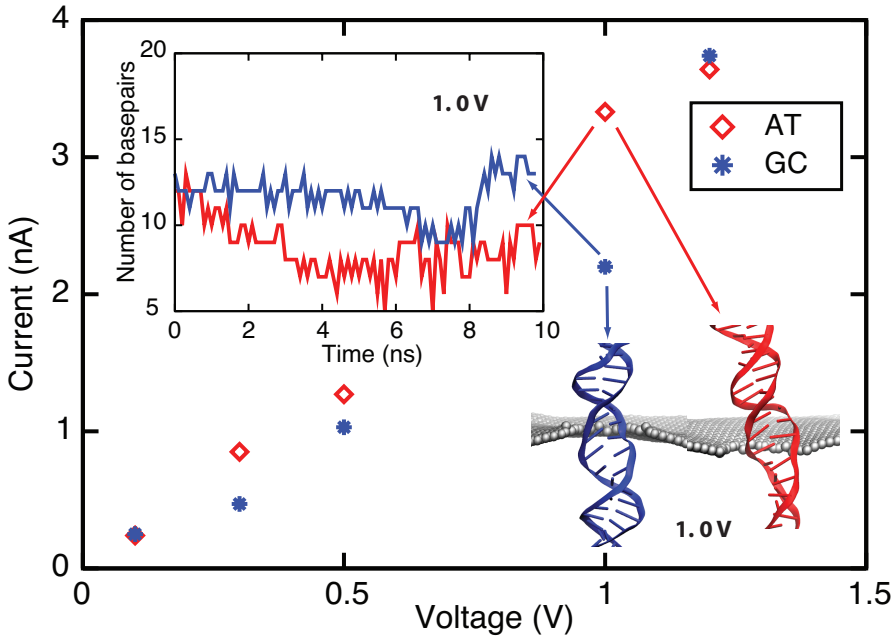

Figure 2.9: Ionic current for poly(A-T)$_{20}$ and poly(G-C)$_{20}$ duplexes measured at 0.1 V, 0.3 V, 0.5 V, 1.0 V and 1.2 V transmembrane bias voltages in a 2.4 nm diameter nanopore (SimE1-SimF5). Translocation of A-T and G-C base pairs results in different ionic currents at 0.3 V, 0.5 V and 1.0 V. The snapshot shows that poly(A-T)$_{20}$ (red) is more stretched and disordered than poly(G-C)$_{20}$ (blue) at 1.0 V. The inset shows the number of base pairs near the pore mouth ($\pm$2 nm): A-T base pairs are more readily broken than G-C base pairs at 1.0 V. Figure 2.10 shows the number of base pairs near the pore mouth for 0.1 V, 0.3 V, 0.5 V and 1.2 V.

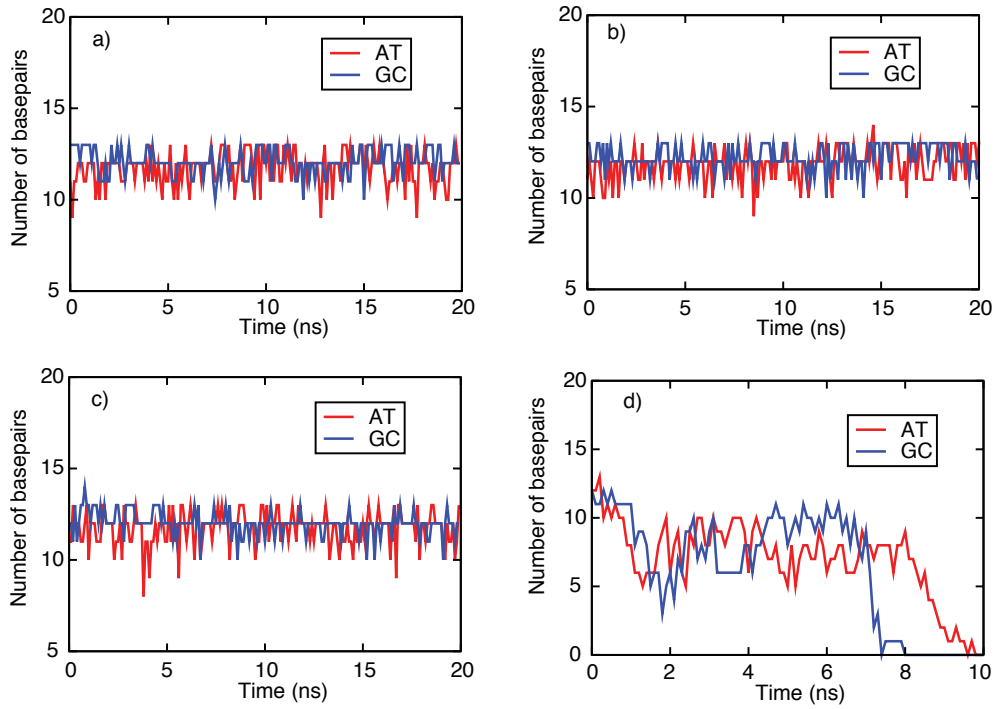

Figure 2.10: Number of base pairs near the pore mouth (±2 nm) for (a) 0.1 V, (b) 0.3 V, (c) 0.5 V and (d) 1.2 V.

pairs in poly(A-T)$_{20}$ and poly(G-C)$_{20}$ tilt in the pore mouth. Poly(A-T)$_{20}$ tilts slightly more than does poly(G-C)$_{20}$, resulting in a slightly larger ionic current. At 1.0 V, the base pairs in poly(A-T)$_{20}$ are more readily stretched and broken than those in poly(G-C)$_{20}$ (see snapshots in Figure 2.9), because an A-T base pair has one intermolecular hydrogen bond less than the G-C base pair. At 1.2 V the base pairs in poly(A-T)$_{20}$ and poly(G-C)$_{20}$ are mostly broken when they pass through the pore mouth (see Figure 2.10) and, therefore, the values of the associated ionic currents are the same. Sequencing dsDNA using nanopores requires, at a minimum, discrimination between A-T and G-C base pair ionic current blockades. Our simulations suggest that it is possible to detect different base pair configurations in dsDNA using an appropriate voltage bias.

2.8 Conclusions

Prior experiments already have been successful in detecting dsDNA molecules using graphene nanopores [30, 31, 32], suggesting graphene to be a new promising material for cheap, rapid DNA sequencing with nanopore technology. To achieve single-base resolution, development of graphene-based DNA sequencing devices requires atomic scale pictures of the kinetics of DNA translocation and concomitant ion currents through the graphene nanopore. In this study, we have provided such detailed picture employing molecular dynamics simulations as a computational microscope. Simulations reveal how ionic current blockades strongly correlate with the local conformation of DNA inside the pore, linking the prior experimental observations to the underlying molecular mechanisms.

A key result of our study is that the size of the pore affects the distribution of the electrostatic potential in the system: for small pores ($d \leq 3$ nm) most of the potential drop occurs near the membrane; the potential drop broadens non-linearly for larger pore diameter ($d \geq 4$ nm), suggesting that DNA molecules can be more readily captured by a larger pore than by a smaller pore beyond the effect expected by pore area only.

Another key result is that pore charge can be used to control the kinetics of DNA translocation through a graphene pore. Previous studies reported that functionalized graphene nanopores furnish molecular sieves for ions [68]. Simulations on permeation of DNA through two modified pores, namely a p-charged pore and an n-charged pore, reveal that under identical bias voltage conditions DNA passes through a p-charged pore faster than through an n-charged pore. The difference can be attributed to the change of the effective pore size for DNA translocation. The simulation trajectories clearly demonstrate DNA needing to adopt a stretched conformation to undergo translocation through an n-charged pore.

A third key result is that the force experienced by nucleotides in the pore can be tailored by varying the applied electric bias voltage to discriminate poly(A-T)$_{20}$ and poly(G-C)$_{20}$. Our simulations are only a first step in studying the feasibility of actual DNA sequencing using graphene

nanopores, raising the possibility of implementing nanopore DNA sequencing using graphene. However, there are many hurdles on the route towards achieving this experimentally [29, 67].

The use of graphene nanopores for DNA sequencing, as suggested here, would require avoiding DNA adherence to the graphene sheet in order to keep DNA stretched in the pore; such avoidance can be realized, keeping the DNA stretched, by using, e.g., optical tweezers. Undulating stretched DNA inside a nanopore using an AC field might exhibit sequence-dependent hysteresis in graphene based nanopores as it does in silicon nanopores [69]. Future studies might focus also on sequence-dependent translocation characteristics of single stranded DNA which was not investigated here due to lack of observational data. In addition to being a sequencing tool, graphene nanopores may also be used for single-molecule force spectroscopy, e.g., to examine the binding force and energy of protein-DNA complexes at a single-molecule level [5, 70].

We note that the π electrons in the graphene membrane are delocalized and, hence, can be readily polarized by the charged DNA and ions passing through the nanopore. Our present simulations do not account yet for such polarization, but they can be extended following the scheme used in the case of carbon nanotubes [52, 71]. It is highly desirable to account for such polarization in future modeling, not only because it affects the force experienced by DNA inside the graphene membrane, but also since the polarization can be possibly used as a signal to further identify a passing DNA sequence. Electronic properties of graphene based nanopores can be tailored by employing bilayer graphene membranes, which have tunable bandgaps [33, 72, 73, 74, 75], and graphene nanoribbons [76], which can further increase the role of the membrane in electrically sensing and controlling the translocation process.

In summary, our MD simulations illustrate at an atomic level that magnitude and duration of the ionic blockade current in graphene nanopores with passing DNA can identify the local configuration of DNA, e.g., the extent of stretch, inside the pore as well as the composition of DNA. The geometry of DNA inside the pore depends on external voltage, the physical and chemical

properties of the pore as well as on DNA sequence. Understanding the influence of each factor on the ionic blockade current signature stemming from translocation of DNA will provide guidance in the design of graphene-based DNA sequencing devices and single molecule sensors.

CHAPTER 3

GRAPHENE QUANTUM POINT CONTACT TRANSISTOR FOR DNA SENSING

3.1 Introduction

Graphene nanoribbons (GNR) are strips of graphene with a finite width that quantizes the energy states of the conduction electrons [77]. Unlike traditional quantum wells, the boundary conditions of GNRs are complicated functions of position and momentum resulting from the dual sublattice symmetry of graphene, giving rise to a unique band structure. Because of this, the shape of the boundary as well as the presence of nanopores profoundly affects the electronic states of GNRs [78], for example, leading to a difference in band structure for zigzag and armchair-edged GNRs [79].

The edge of a GNR can be patterned with near-atomic precision, opening up the possibility to investigate many different geometries. In the case of complicated edge shapes, the current displays an extremely nonlinear and not strictly increasing dependence on carrier concentration. The graphene Quantum Point Contact (g-QPC) is a perfect example in this regard, as its irregular edge yields a complex band structure and rich conductance spectrum with many regions of high sensitivity and negative differential transconductance (NDTC). In addition, the g-QPC electronic properties are not limited by stringent GNR uniformity (armchair or zigzag) in the boundary conditions. Moreover, the carrier concentration itself, which can be controlled by the presence of a back-gate embedded within a g-QPC device as in a field-effect transistor (FET), can profoundly affect the sensitivity and nonlinearity of the current. As a result, changes in external electric fields, including changes

due to rotation and translation of external molecular charges, alter the local carrier concentration and can dramatically influence the g-QPC conductance. In the following we demonstrate the complex and nonlinear effects of altering boundary shapes, graphene carrier concentrations, and electric potentials due to DNA translocation on the conductance of such a device. We propose to sense DNA by performing transport measurements in a g-QPC device and demonstrate that the sensitivity of the conductance can be geometrically and electronically tuned to detect small differences in the charge geometry of biomolecules such as DNA.

3.2 Structure description

Figure 3.1 shows a monolayer g-QPC device in an ionic water solution, containing a single layer of patterned graphene connected to source and drain leads and sandwiched between two oxide layers to isolate the graphene from the aqueous environment. The graphene and oxide layers have coaxial nanopores ranging from 2 to 4 nm, allowing charges, molecules, or polymers to pass through. Critical to the device shown is a back gate underneath the lower oxide substrate made of a metal or heavily-doped semiconductor or another graphene layer to control the charge carrier concentration in graphene as in a field-effect transistor configuration; the back gate enhances its electrical sensitivity to DNA translocation. The diameter of the nanopore is small enough to attain the required sensitivity, but is wide enough to let the biomolecules translocate.The diameter of the nanopore is small enough to attain the required sensitivity, but is wide enough to let the biomolecules translocate.

In this study, we investigate four edge geometries, namely a 5 nm wide and a 15 nm wide pure armchair-edge GNR as well as an 8 nm wide and a 23 nm wide QPC edge. These geometries will herein be referred to as 5-GNR, 15-GNR, 8-QPC, and 23-QPC. The QPC geometries have pinch widths of 5 nm and 15 nm (2/3 total width), the same as the widths of the armchair-edged GNRs.

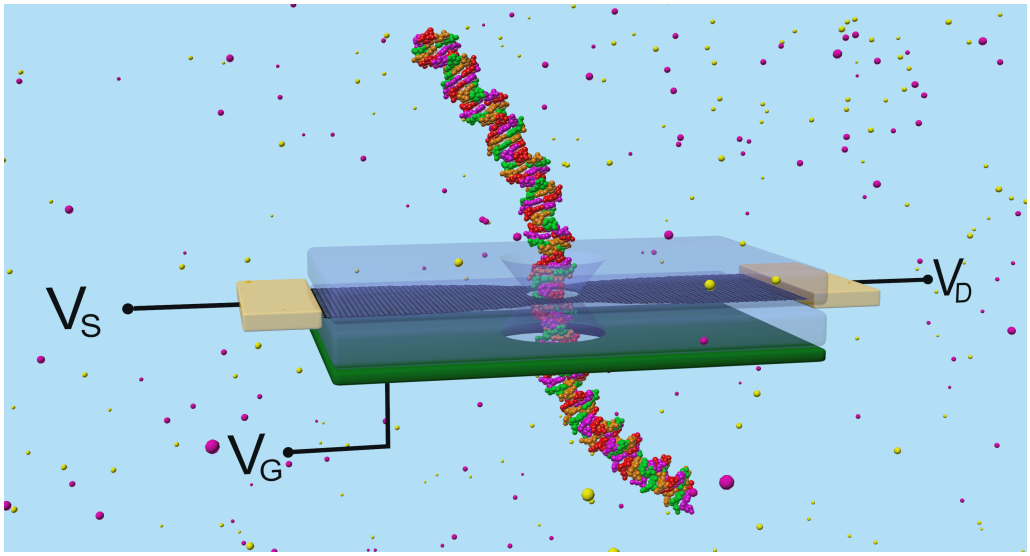

Figure 3.1: Schematic diagram of a prototypical solid-state, multilayer device containing a GNR layer (black) with a nanopore, sandwiched between two oxides (transparent) atop a heavily doped Si back gate, V_G (green). The DNA is translocated through the pore, and the current is measured with the source and drain leads, V_S and V_D (gold).

3.3 Methods

3.3.1 Self-consistent determination of electric potential

In order to determine the electronic transport properties of the QPC GNRs, we first obtain the electrostatic potential on the GNR due to external charges in the DNA molecule as well as in the electrolytic solution from each trajectory snapshot. We self-consistently solve the Poisson equation for a 3D box containing the graphene membrane, DNA molecule, and ions immersed in solution with a Newton-multigrid method to obtain the electric potential $\phi(\boldsymbol{r})$ [80]

$$\boldsymbol{\nabla} \cdot [\epsilon(\boldsymbol{r}) \boldsymbol{\nabla} \phi(\boldsymbol{r})] = -e[K^+(\boldsymbol{r}) - Cl^-(\boldsymbol{r})] - \rho_{fixed}(\boldsymbol{r}) \tag{3.1}$$

Here, ϵ is the local permittivity. The right-hand-side charge term includes ions in solution (K^+,Cl^-) and fixed charges ρ_{fixed} such as DNA charge present in the system. We assume the electrolyte distributions obey Boltz-

mann statistics [3]

$$K^+(\boldsymbol{r}) = c_0 \exp[-\frac{e\phi(\boldsymbol{r})}{k_B T}], \quad Cl^-(\boldsymbol{r}) = c_0 \exp[\frac{e\phi(\boldsymbol{r})}{k_B T}] \tag{3.2}$$

Here, K^+ and Cl^- are the local ion concentrations, e is the electronic charge, and c_0 is the molar concentration of KCl. We assume the base concentration is 1 M. The system is discretized onto a nonuniform $256 \times 256 \times 256$ point grid, with a higher grid resolution around the graphene nanopore region. Neumann boundary conditions are imposed on the sides of the box, while the top of the box is subject to a Dirichlet boundary condition $V_{TOP} = 0$.

Once Eq. 3.1 is solved, the resulting potential in the nanopore graphene layer can be used to calculate its carrier concentration and transport properties.

3.3.2 Electronic transport properties of graphene nanoribbons

For this purpose we use a formalism based on the tight-binding approximation, in which the Hamiltonian for a graphene nanoribbon can be written as [81]

$$H = \sum_{i,\mu} [\epsilon_\mu - e\phi(\boldsymbol{r_i})] a_i^{\mu\dagger} a_i^\mu + \sum_{\substack{<ij> \\ \mu\nu}} V_{\mu\nu}(\vec{n}) a_i^{\mu\dagger} b_j^\nu + V_{\nu\mu}(\vec{n}) b_j^{\nu\dagger} a_i^\mu \tag{3.3}$$

where e_μ is the on-site occupation energy of an electron in state μ located at site i, e is the magnitude of the electronic charge, $\phi(\boldsymbol{r_i})$ is the electric potential at site i obtained from Eq. 3.1, and $a_i^{\mu\dagger}/b_i^{\mu\dagger}$ and a_i^μ/b_i^μ create and annihilate electrons in state μ at site i for the graphene A/B sublattice, respectively. The states μ, ν are superpositions of the p_z, d_{yz}, and d_{zx} orbitals of monatomic carbon as opposed to solely including the p_z orbital in traditional tight-binding models of graphene. This expanded basis improves the accuracy of the electronic structure as well as allowing for the inclusion of edge-passivation. The values of the transfer integrals $V(\vec{n})$ are determined by fitting these parameters to ab initio calculations and depend on $\vec{n}$, the unit displacement between sites i and j. The values for all on-site energies and transfer integrals are taken from [81].

Once the Hamiltonian is determined, the electronic properties of the graphene nanoribbon can be calculated by using the Non-Equilibrium Green's Functions (NEGF) technique. The Green's function $\boldsymbol{G}$ is given in the operator representation as

$$\boldsymbol{G}(E) = [E - \boldsymbol{H}]^{-1} \tag{3.4}$$

or in real space

$$[E \pm i\eta - H(\boldsymbol{r}, \boldsymbol{r'})]G(\boldsymbol{r}, \boldsymbol{r'}) = \boldsymbol{\delta}(\boldsymbol{r} - \boldsymbol{r'}) \tag{3.5}$$

where $\boldsymbol{H}$ is the Hamiltonian of the system and η is infinitesimally small. If we discretize the real space coordinates to correspond to positions on the lattice, we can divide the device into three sections, two leads (L) on either side of a conductor (C).

$$\begin{bmatrix} G_L & G_{LC} & 0 \\ G_{CL} & G_C & G_{LC} \\ 0 & G_{CL} & G_L \end{bmatrix} = \begin{bmatrix} E - H_L & V_{LC} & 0 \\ V_{CL} & E - H_C & V_{LC} \\ 0 & V_{CL} & E - H_L \end{bmatrix}^{-1} \tag{3.6}$$

If $V_{LC} = V_{CL}^{\dagger}$, Eq. 3.6 yields

$$G_C = [(E + i\eta)I - H_C - \sum_{\alpha} \Sigma_{\alpha}]^{-1} \tag{3.7}$$

where $\Sigma_{\alpha} \equiv V_{\alpha C}^{\dagger}[E - H_{\alpha}]^{-1}V_{\alpha C}$ is the self-energy of lead α. For modeling different conductors with identical leads, $[E - H_{\alpha}]^{-1}$ only needs to be calculated once.

The transmission function, which is used to find the conductance, can be determined from the Green's function. The transmission $\bar{T}(E)$ between the leads 1 and 2 is given by [82]

$$\bar{T}_{12} = -Tr[(\Sigma_1 - \Sigma_1^{\dagger})G_C(\Sigma_2 - \Sigma_2^{\dagger})G_C^{\dagger}] \tag{3.8}$$

The conductance across the conductor at a particular bias V_{DS} can be expressed as

$$G = \frac{2e}{V_{DS}h} \int_{-\infty}^{\infty} \bar{T}(E)[f_1(E) - f_2(E)]dE \tag{3.9}$$

where $f_\alpha(E) = f(E - \mu_\alpha)$ is the probability an electron occupies a state at energy E in the lead α, $\mu_1 - \mu_2 = V_{DS}$ is the bias across the conductor. μ_1 is taken to be the Fermi energy of the conductor. In all subsequent calculations it is assumed that $f(E)$ is the Fermi-Dirac distribution function and the temperature is 300 K.

3.4 Conductance variations due to external charges

The effect of a test charge, placed within a pore, on electronic transport in graphene is illustrated in Figure 3.2. Shown are the conductance changes upon placing a single electron charge (e) at two positions within a 2 nm pore at P; one position is at 1/2 radius to the west of the pore center (W or west) and the other at 1/2 radius south of the pore center (S or south). Figures 3.2a and b display the conductance response for the 5-GNR and 15-GNR respectively, while Figure 3.2c and d display conductance responses for the 8-QPC and 23-QPC, respectively. The difference in conductance upon charge placement varies between 0 and 0.8 μS for all geometries, which is well within the sensing range of most current probes. Conductance change for the 5-GNR (Figure 3.2a) are negligible over most of the energy range for both angular charge (W and S) positions, due to the suppressed transmission probability at low carrier energies. For the 15-GNR, 8-QPC, and 23-QPC cases (Figure 3.2b, c, and d) the angular position of the charge within the pore has a significant effect on the conductance, causing not only large differences in conductance over the investigated energy range but also a different sensitivity of the conductance to the Fermi energy. In these cases, the maximum difference in conductance occurs for a test charge in the west (south) position at smaller (larger) Fermi energies. The conductance can be either enhanced or reduced by the test charge, depending on the value of the Fermi energy. In the case of the 15-GNR (Figure 3.2b), for example, when the Fermi energy lies between 0 and 0.18 eV, the conductance change for the electron test charge in the west position is positive, while the change is negative for Fermi energies above this range. Similar behavior is seen for the

8-QPC and 23-QPC, but over different Fermi energy ranges (Figures 3.2c and d).

One also notes that in Figure 3.2, for all cases, the differences in conductance are anti-symmetric with respect to the Fermi energy. This is a direct consequence of the symmetry between electrons and holes in graphene. Because of this symmetry, electrons and holes tend to react to the same potential with opposite sign, such that the conductance changes are an odd function of Fermi energy. For instance, in Figure 3.2b, there is a peak in the conductance change for the 15-GNR around 0.1 eV for all four charge configurations; a similarly shaped peak, but with opposite sign, is located at -0.1 eV. Similarly, one finds for the 23-QPC, as shown in Figure 3.2d, peaks at 0.15 eV and opposite peaks at -0.15 eV. The reader can notice, however, the different parity between the differential conductance curves at low energy in Figures 3.2c and d, which are negative for the 8-QPC (Figure 3.2c) and positive for the 23-QPC (Figure 3.2d).

3.5 Electrical response to DNA translocation

In order to demonstrate a potential application of a charge-sensing device exploiting the sensitivity of geometrically-tuned GNRs, we simulated the translocation of a strand of DNA through a 2.4 nm pore located at the center (point P above) of the four edge geometries. We translocate a 24 base pair B-type double-stranded DNA segment consisting of only AT nucleotide base pairs. The DNA is initially placed such that the bottom of the strand is 3.5 Å above the graphene membrane, and the axis of the DNA passes through the center of the nanopore (Figure 3.3a). The DNA is then rigidly translocated through the nanopore at a rate of 0.25 Å per time step (snapshot) until the DNA has passed through the pore completely. After the last (400th) snapshot the top of the DNA strand is 13.5 Å below the graphene membrane. The charge distribution from the DNA at each time step (snapshot) is mapped into the Poisson solver, and the electric potential on the graphene membrane is calculated for each snapshot as the DNA rigidly translocates through the pore. Due to strong screening from ions and water

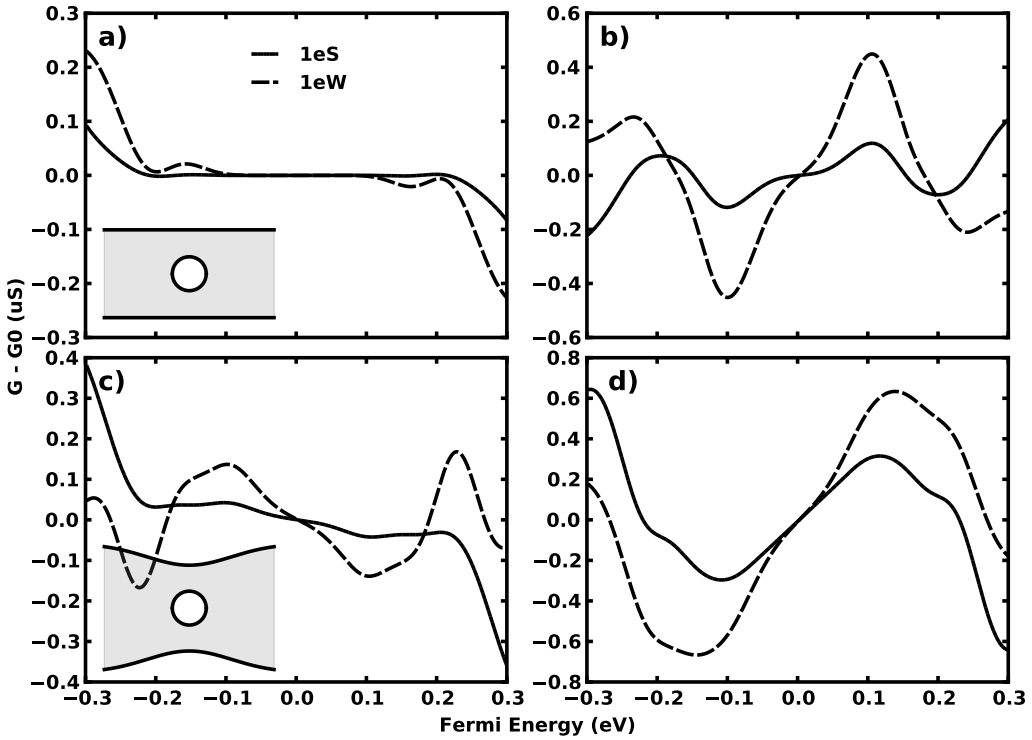

Figure 3.2: Change in the conductance due to adding an external charge within the 2 nm pore. "S" means the charge is placed one half radius south of the center of the pore, and "W" means the charge is placed one half radius west of the center of the pore. (a) 5-GNR, (b) 15-GNR, (c) 8-QPC, and (d) 23-QPC.

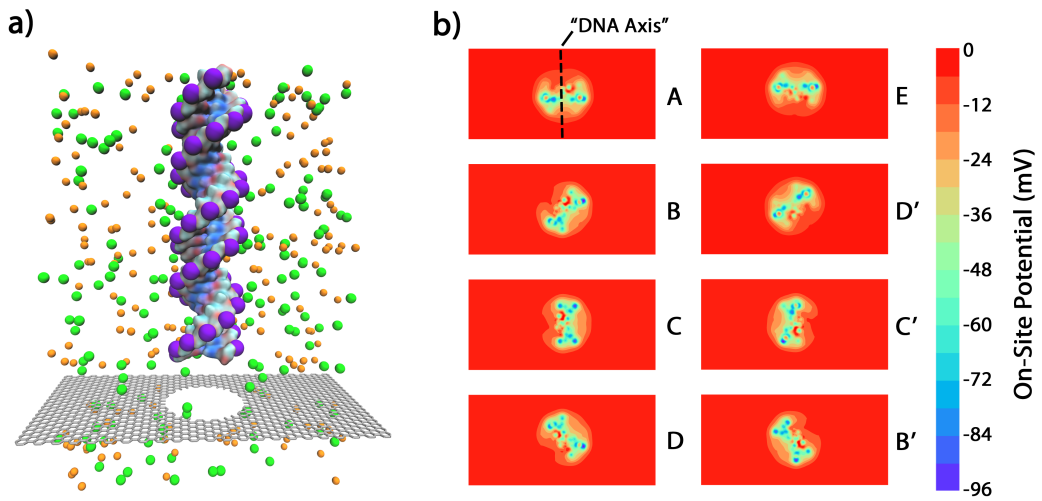

Figure 3.3: (a) Schematic of an AT DNA strand translocating through a pore. (b) Potential maps in the graphene plane due to the DNA molecule at eight successive snapshots throughout one full rotation of the DNA strand.

near the graphene membrane, the on-site electric potential of the nanopore is dominated by charges contained within a slice coplanar with the graphene membrane and directly inside the nanopore. Hence, during the translocation of the biomolecule through the nanopore, the graphene membrane will sense a succession of DNA slices, which appear as an in-place rotation of the double helix in the absence of translocation. Since it is only the charges in the pore that matter (due to the strong screening effects), the electric potentials around the pore due to the DNA being pulled through are virtually identical to the potential arising if the DNA slice coplanar with the membrane was rotated without translocation. Figure 3.3b shows the on-site potentials for eight successive positions of the DNA (A-B-C-D-E-D-C-B) in the graphene plane, representing one half cycle of this pseudo-rotational behavior.

As mentioned above, the lattice including a nanopore may not be both x-axis and y-axis reflection symmetric with the pore at the center due to the discrete nature of the lattice. For example, the 15-GNR with a 2.4 nm pore exhibits y-axis reflection symmetry, but not x-axis reflection symmetry, as in the shape of the letter "Y." In contrast, the 5-GNR, 8-QPC, and 23-QPC geometries with a 2.4 nm pore exhibit both y-axis and x-axis reflection symmetry, as in the shape of the letter "X." These symmetries have an effect

on the electronic conductance in GNRs when the DNA strand is introduced. When calculating the conductance from the transmission probability, it is important to note that the transmission probability itself does not represent a particular direction of current flow. In other words, a reflection about either the x- or y-axis of the lattice and its on-site electric potential map leaves the transmission probability, and hence the conductance, unchanged. When the DNA strand is translocated, the electric potential maps of successive snapshots look like A->B->C->D in Figure 3.3b corresponding to the translocation of one half pitch of the DNA helix, and for the second half of the cycle the successive snapshots look like E->D->C->B. The D, C, and B potential maps are effectively the mirror images (y-axis reflected) of D, C, and B, respectively. As a result, assuming the DNA potential is reflection symmetric about its own axis "DNA axis"), the conductance curves corresponding to geometries with only y-axis reflection symmetry should display a half-cycle "mirror" effect, repeating only after a full A->E->A rotation, i.e. the conductance should be identical for snapshots D and D, C and C, etc. On the other hand, because the electric potential maps B and D (and therefore B and D) are identical after an x-axis reflection, the conductance should mirror after a quarter-cycle translation of the DNA and should repeat itself after a half-cycle (A->B->C->D) in the 5-GNR, 8-QPC, and 23-QPC.

Figurse 3.4a-d show the conductance as a function of the snapshot number (time) for Fermi energies 0.04 eV, 0.08 eV, 0.12 eV, and 0.16 eV above the Dirac point for each of the four geometries with a 2.4 nm pore at point P. The lines marked A-B-C-D-E-D-C-B correspond to the eight potential maps in Figure 3.3b, representing the translation of one full helix of the DNA. As can be seen in Figure 3.4b, the 15-GNR displays the half-cycle mirroring behavior described above, only repeating after each full helix translocates through the pore. On the other hand, the 5-GNR, 8-QPC, and 23-QPC conductances shown in Figures 3.4a, c, and d respectively, display the quarter-cycle mirror effect; lines A-C represent one quarter of the helix, C-E represent the second quarter, etc. The DNA molecule in Figure 3.3a, contains 24 AT base pairs, which give rise to 2.5 full turns of the double-helix. As a result, full translocation of the DNA molecule should result in 2.5 periods in the conductance curves of the 15-GNR, and five periods in the case of 5-GNR, 8-QPC and 23-QPC which is indeed the case as shown in Figure 3.4. In these latter

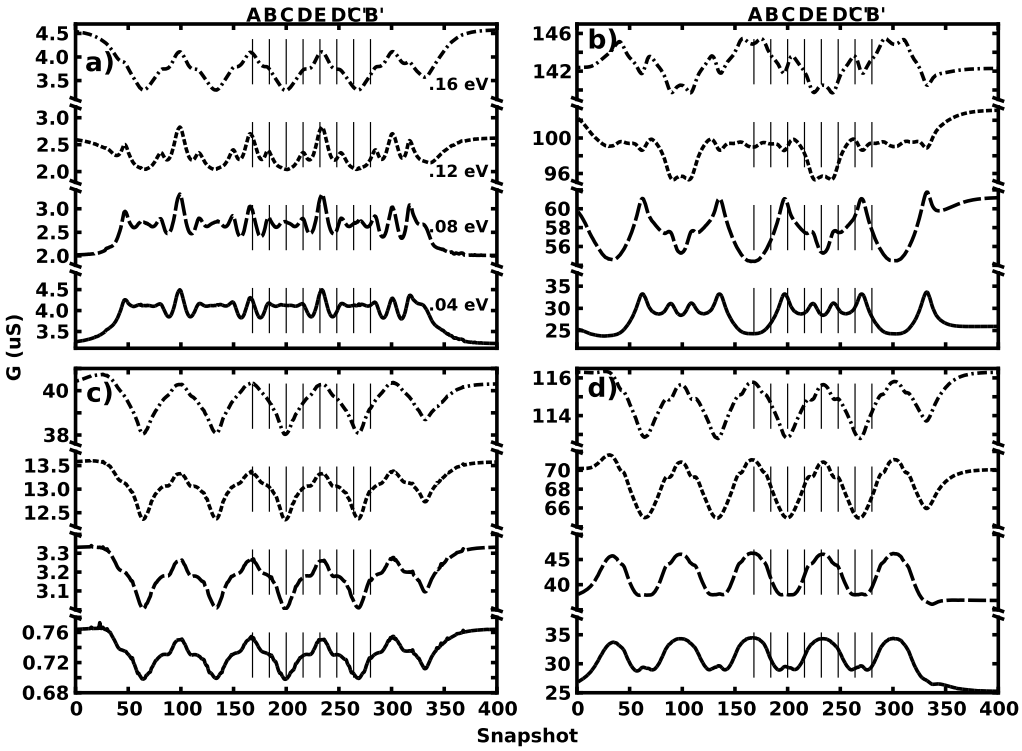

Figure 3.4: Conductance as a function of DNA position (snapshot) for multiple Fermi energies, 0.04 eV (solid), 0.08 eV (long dash), 0.12 eV (short dash), and 0.16 eV (dot dash), as the DNA strand rigidly translocates through a 2.4 nm nanopore pore located at the device center (point P). (a) 5-GNR, (b) 15-GNR, (c) 8-QPC, and (d) 23-QPC.

conductance curves, the peaks of each cycle correspond to potential map A, when the DNA axis is parallel to the y-axis, while the troughs correspond to potential map C, when the DNA axis is parallel to the x-axis. The DNA molecule is not perfectly symmetric, as the bases in a base pair are different nucleotides; additionally, there may be a small discretization asymmetry in the potential map of the DNA. The cumulative effect is a slight difference in the conductance after a y-axis reflection, which can be recognized in Figures 3.4a, c, and d.

The large conductance variations accompanying DNA translocation through the pore demonstrate the high sensitivity of the device to external charges and their conformation. With a source-drain bias of 5 mV, the conductance (current) displays maximum variations of 0.8 to 8 μS (4 to 40 nA) depending on the particular geometry (Figure 3.4), well detectable with present technology. These large variations reinforce the idea that angular position and Fermi level, in concert with each other, can strongly change the magnitude of the electrical sensitivity of the devices. Additionally, for some geometries, such as the 8-QPC (Figure 3.4c), a small change in Fermi energy (0.12 eV to 0.16 eV) results in a threefold change in the magnitude of the conductance (13 μS to 40 μS) and a threefold increase in the magnitude of conductance variations (0.9 μS to 2.8 μS). Interestingly, because of the presence of NDTC regions within the investigated Fermi energy range, an increase of Fermi energy may actually decrease the conductance, as in case of the 5-GNR (Figure 3.4a). Studies on electrochemical activity at the edge of graphene nanopore have been reported recently [83] which can lead to an electrochemical sheet current in graphene of the order of 0.5 nA for a pore diameter of 2.4 nm. Although this is a large electrochemical current, the sensitivity reported here to DNA translocation is much larger than the electrochemical current measured, especially at larger Fermi energies.

In our simulation, a new nucleotide is within the plane of the nanopore after thirteen time steps. However, no such periodic modulation is visible in the conductance curves of Figure 3.4. The reason for this is the strong screening due to the phosphate backbone on the DNA strand. As a result, the conductance variation reflects the positional changes of the backbone charges as opposed to the movement of the nucleotide charges themselves.

In order to sequence DNA, one must be able to detect these nucleotides, either by translocating a single strand of DNA to prevent screening of the nucleotides by the backbone, or by making the DNA and its backbone undergo nucleotide-specific conformational changes, a topic which we are currently investigating as well as the influence of the thermal fluctuations of the DNA molecule on the g-FET conductance.

3.6 Conclusion

In this chapter a new strategy for sensing the molecular structure of biomolecules by using a nanopore in electrically active mono-layer graphene shaped with a lateral constriction or QPC, employing an electrically tunable conductance to optimize detection sensitivity. The suggested measurement has been analyzed theoretically by using a self-consistent model that integrates the NEGF formalism for calculating electronic transport in the g-QPC with a detailed description of the electrical potential due to solvent, ions, and molecular charges in the nanopore. In particular, we have demonstrated that graphene QPCs are capable of detecting DNA molecules translocating through the nanopore, with a sensitivity controlled by the graphene carrier concentration. In order to achieve QPC carrier tunability, we propose a solid-state membrane design made of a graphene QPC sandwiched between two dielectrics to isolate the active g-layer from the electrolyte as well as suppress mechanical fluctuations of the membrane itself; the design permits simultaneous control of the carrier concentration by an external gate as in a field-effect transistor configuration feasible with modern semiconductor technology.

CHAPTER 4

ELECTRONIC DETECTION OF DSDNA TRANSITION FROM HELICAL TO ZIPPER CONFORMATION USING GRAPHENE NANOPORES

4.1 Introduction

Study of the mechanical properties of DNA, enabled by single-molecule experiments, is essential to understanding many key biological processes such as DNA transcription, packing, and replication. The ability to manipulate the structure of DNA at the nanoscale and change DNA electronic and mechanical properties has led to synthetic DNA-based nanodevices [84]. For example, the mechanical structure of a DNA molecule can be manipulated using an atomic force microscope (AFM), where one end of the DNA is tethered to a glass surface and the other end is attached to the AFM cantilever. Displacement of the cantilever exerts a force on the DNA molecule and thereby stretches it [85, 86, 87]. Optical tweezers [88], magnetic tweezers [89] and nanopores [3, 13, 90, 91] likewise can be used to trap DNA molecules and stretch them. Forced extension of double-stranded DNA (dsDNA) transforms its structure from a canonical helical conformation (B-DNA) to a stretched conformation (S-DNA) [92]. The S-DNA can further take a zipper-like form (zip-DNA), where complementary base pairs, on the two strands, are broken and interdigitate giving a zipper-like resemblance [93, 94].

In the present chapter, we demonstrate that the change in dsDNA conformation arising in the so-called B-DNA to zip-DNA transition can be detected through transverse electronic conductance, which arises in a graphene nanopore translocating the DNA and being employed as a sensor. To achieve such detection, we performed molecular dynamics simulations to induce forced B-DNA to zip-DNA extension in a 15-bp-long helical dsDNA, i.e., B-DNA, and observed a structural transition from helical to zipper form. The conductance in a graphene membrane was shown to be affected by the different

dsDNA conformations arising during the B to zip transition. For this purpose the structures arising in the molecular dynamics simulations were used to determine the electrostatic potential around the dsDNA and the result fed into NEGF calculations of the graphene membrane conductance. The conductance changed from an oscillating type response, at the B-DNA stage, to a constant conductance corresponding to the zip-DNA stage. The capability of detecting conformational changes in dsDNA using transverse electronic conductance can complement ionic current measurements and potentially extend the molecular sensing capability of graphene-based nanopores.

4.2 Model and methods

Steered molecular dynamics (SMD) simulations were employed to induce forced extension of dsDNA from B-form to zip-form. The simulations were performed on poly(A-T)$_{15}$ and poly(G-C)$_{15}$ strands with the DNA placed in a water box of size 70 Å×70 Å×110 Å and neutralized at 1 M KCl, amounting to 357 K^+ and 327 Cl^- ions. The simulated systems contained about 52,000 atoms. To accommodate the molecular extension along the z-axis the length of the water box was chosen twice as large as the initial length of the DNA, whose axis was aligned along the z-direction. The simulated system is shown in Figure 4.1a. To gain better sampling of the force-induced extension five independent SMD simulations were performed on both poly(A-T)$_{15}$ and poly(G-C)$_{15}$ strands.

All molecular dynamics simulations were carried out using NAMD 2.9 [49], employing periodic boundary conditions, with the CHARMM27 force field parameters for dsDNA [51], ions and employing the TIP3P water model [53]. The dsDNA was built using the program X3DNA [50] and the topology of dsDNA along with the missing hydrogen atoms were generated using psfgen [49]. The system was energy minimized for 4000 steps, then heated to 295 K in 4 ps. A 0.5 ns equilibration under NPT ensemble conditions was performed to equilibrate the system to a desired pressure of 1 atm. This equilibration step was followed by a 1.5 ns equilibration under NVT ensemble condition. A temperature of 295 K was maintained by applying Langevin dynamics with a damping constant of 0.2 ps^{-1}; constant pressure

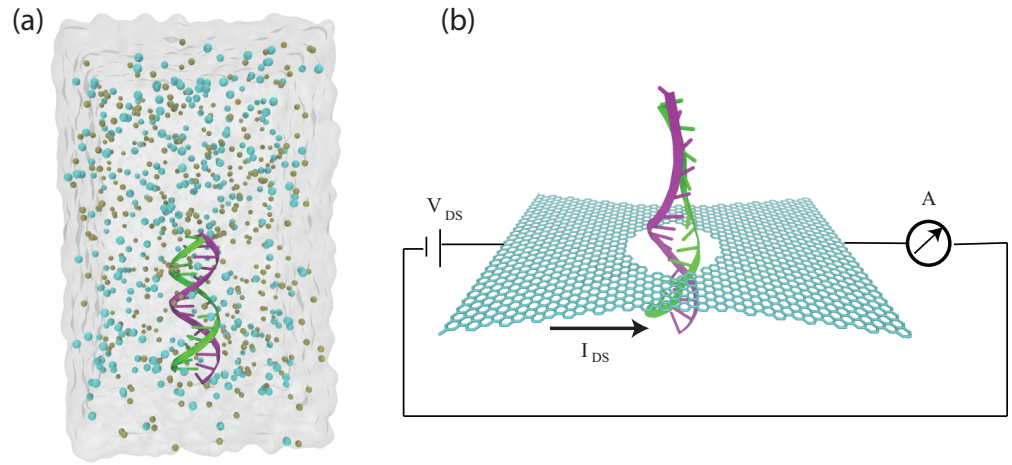

Figure 4.1: Model of the simulated system. (a) All-atom MD model comprising of a 15-bp-dsDNA, K^+ and Cl^- ions, and water box. The dimensions of the simulated periodic cell were 70 Å×70 Å×110 Å. (b) Schematic of graphene nanopore system used to calculate the transverse electronic conductance. Shown in the figure is the snapshot of a DNA conformation that arose during one of the MD simulations. The DNA being extended was placed after the actual MD simulations inside a QPC edge nanopore to mimic an actual translocation process through the pore. The electrostatic potential surrounding the DNA was calculated and fed into a NEGF calculation of the transverse electronic conductance induced by the potential in the graphene membrane. A pore diameter of 2.4 nm was assumed.

of 1 atm was maintained using a Nośe-Hoover Langevin piston barostat [54] with a period and decay of 200 fs; long-range Coulomb interactions were computed using the particle-mesh Ewald (PME) method with a grid size of < 1 Å; van der Waals interactions were calculated using a 12 Å cuttoff; an integration timestep of 1 fs was adopted, with a multiple timestepping algorithm [95, 96] employed to compute the bonded interactions at every timestep, the short-range non-bonded interactions every other timestep, and the long-range electrostatic forces every fourth timestep (employing so-called 1-2-4 timestepping). SMD simulations were then performed by harmonically restraining both, 3' and 5', terminal phosphate atoms on one end, while applying an external force to the corresponding atoms at the other end at a constant velocity of 1 Å/ns, along the z-direction, to induce forced extension

of dsDNA. A 2 fs integration timestep was adopted for SMD simulations with a 2-1-2 multiple timestepping scheme. The covalent hydrogen bonds in DNA and water were constrained using RATTLE [97] and SETTLE [98] algorithms, respectively. Each independent SMD simulation was 60 ns long, covering a total simulation time of 0.6 μs for five independent trajectories for each poly(A-T)$_{15}$ and poly(G-C)$_{15}$.

The electrostatics surrounding the DNA shifted through the graphene nanopore was described using the Poisson-Boltzmann equation

$$\nabla \cdot [\epsilon(\vec{r})\nabla\phi(\vec{r})] = -e[K^+(\vec{r},\phi) - Cl^-(\vec{r},\phi)] - \rho_{DNA}(\vec{r}) \tag{4.1}$$

where $\phi(\vec{r})$ is the electrostatic potential and $\epsilon(\vec{r})$ is the local permittivity. The three-dimensional charge distribution due to the DNA, $\rho_{DNA}(\vec{r})$, was obtained from a prior MD trajectory. The ion solution obeyed Boltzmann statistics, namely [3]

$$K^+(\vec{r},\phi) = c_0 \exp(-e\phi/k_{\mathrm{B}}T), \quad Cl^-(\vec{r},\phi) = c_0 \exp(e\phi/k_{\mathrm{B}}T) \tag{4.2}$$

Here, $K^+(\vec{r})$ and $Cl^-(\vec{r})$ are the spatial ion concentrations, e is the electronic charge and c_0 is the molarity of the KCl solution (1 M). The nonlinear Eq. 5.1 was solved self-consistently using a Newton multigrid scheme [80] on a three-dimensional space ($L_x \times L_y \times L_z$). The DNA charge density was translocated through a quantum point contact (QPC) edge graphene nanopore (diameter = 2.4 nm), which was placed at $z = L_z/2$ (see Figure 4.1b). Dirichlet boundary conditions, $\phi(z = 0) = \phi(z = L_z) = 0$, were assumed along the z-direction, and Neumann boundary conditions, $\nabla_x\phi(x = 0) = \nabla_x\phi(x = L_x) = \nabla_y\phi(y = 0) = \nabla_y\phi(y = L_y) = 0$, were assumed along the x- and y-directions. The Poisson Eq. 5.1 was discretized on a non-uniform, rectangular, three-dimensional grid consisting of 256 $\times$ 256 $\times$ 256 grid points spanning a volume of $10 \times 8 \times 20$ nm^3, with the mesh size ranging from 1/3 Å near the pore mouth to 1 Å far away from the pore. The dielectric constant of water and graphene were set to 78 and 6, respectively [99].

The electronic structure of graphene around the nanopore was described

using the tight binding Hamiltonian [81]

$$H = \sum_{i,\mu}[\epsilon_\mu - e\phi(\boldsymbol{r_i})]a_i^{\mu\dagger}a_i^{\mu} + \sum_{\substack{<ij>\\ \mu\nu}} V_{\mu\nu}(\vec{n})a_i^{\mu\dagger}b_j^{\nu} + V_{\nu\mu}(\vec{n})b_j^{\nu\dagger}a_i^{\mu} \tag{4.3}$$

where e_μ is the on-site occupation energy of an electron in state μ located at site i, e is the magnitude of the electronic charge, $\phi(\boldsymbol{r_i})$ is the electrostatic potential at site i obtained from the Poisson-Boltzmann Eq. 5.1, and Fermion operators $a_i^{\mu\dagger}/b_i^{\mu\dagger}$ and a_i^{μ}/b_i^{μ} create and annihilate electrons in state μ at site i for the graphene A/B sublattice, respectively. The states μ, ν are described as superpositions of the p_z, d_{yz}, and d_{zx} orbitals of mono-atomic carbon. The values for all on-site energies and transfer integrals are taken from [81].

The conductance across the conductor at a particular bias V_{DS} can be expressed as [82]

$$G = \frac{2e}{V_{DS}h}\int_{-\infty}^{\infty} \bar{T}(E)[f_1(E) - f_2(E)]dE \tag{4.4}$$

where $f_\alpha(E) = f(E - \mu_\alpha)$ is the probability that an electron occupies a state at energy E in the lead α, $\mu_1 - \mu_2 = V_{DS}$ is the bias across the conductor. μ_1 is taken to be the Fermi energy of the conductor, calculated by enforcing charge neutrality in the graphene layer. In our calculations we assumed $f(E)$ to be the Fermi-Dirac distribution, $V_{DS} = 5$ mV and a system temperature of 295 K was adopted. The transmission function $\bar{T}(E)$ was calculated using the NEGF technique as outlined in [82, 100]

4.3 Forced extension of dsDNA

The mechanical response of DNA to external forces can be studied in silico using SMD simulations [101, 102]. Earlier simulation studies investigated force-induced stretching of dsDNA by applying a pulling force to the 5' and 3' termini on one end of the dsDNA and by constraining the corresponding termini at the opposite end, causing the strands to stretch parallely to each other and to undergo the B-DNA to zip-DNA transformation [93, 94, 103]. Simulation studies performed under different pulling conditions, like pulling

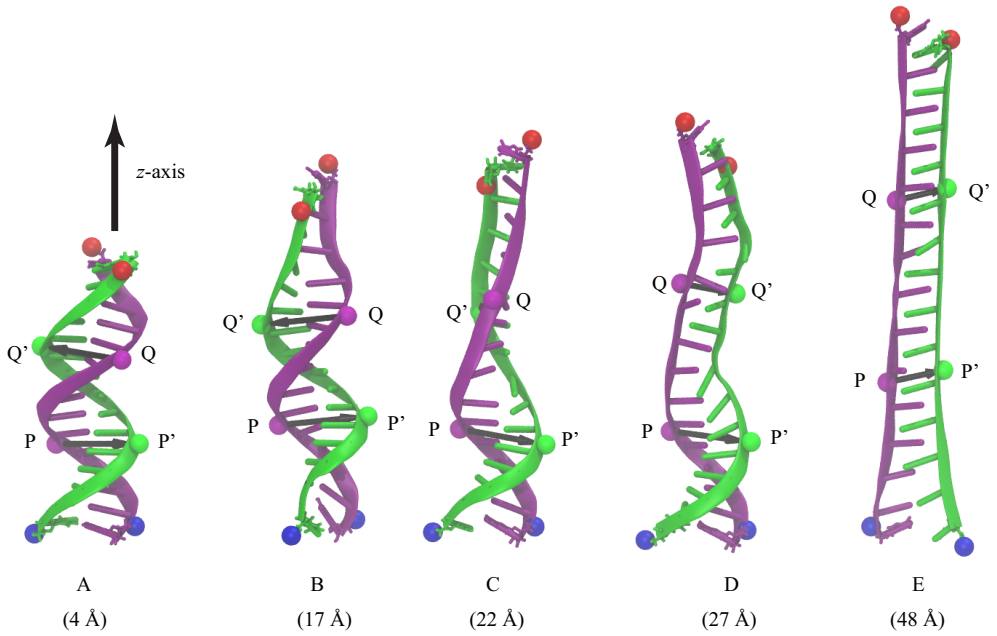

Figure 4.2: Five representative snapshots (A-E) from a single SMD trajectory of poly(A-T)$_{15}$ DNA during a B-DNA (A) to zip-DNA (E) transition. The atoms colored in red were pulled in the z-direction at a rate of 1Å/ns; the blue colored atoms were harmonically restrained to the initial positions. Also shown is the evolution of two sets of base pairs, P-P' and Q-Q', which are a half pitch (namely 5 bp) apart. The black arrows, joining P to P' and Q to Q', initially pointing in opposite directions corresponding to a pure helical conformation (B-DNA) align themselves in the same direction once the zipper conformation (zip-DNA) is reached. The numbers below each snapshot represent the corresponding molecular extension.

the 3' or 5' termini of both strands in opposite directions or torsionally constraining the dsDNA while pulling, can produce more complex structural changes including local DNA melting [104, 105, 106]. Pulling only one of the termini (3' or 5') and constraining the corresponding termini on the opposite end can lead to strand separation. In fact, various types of SMD simulations have been employed to study the effects of methylation and hydroxymethylation on DNA strand separation [107, 108].

In the present study, dsDNA was stretched by pulling both strands on one end of the dsDNA (atoms colored red in Figure 4.2) at a constant velocity of 1Å/ns along the z-direction, while harmonically restraining the other end (atoms colored blue in Figure 4.2). The pulled atoms were attached to one

end of a virtual spring; the other end of the spring, a dummy atom, was moved at a constant pulling speed v (1Å/ns) along the z-direction. The pulled atoms experience a force $f = -k[z(t) - z(t_0) - v(t - t_0)]$, where $z(t_0)$ is the initial position of the dummy atom attached to the spring. The spring constant k was chosen to be equal to $3k_BT_0/Å^2$ (k_B, Boltzmann constant; $T_0 = 295$ K), which corresponds to a thermal RMSD deviation of $\sqrt{k_BT_0/k} \approx 0.6$ Å, which is typical for SMD simulations [101, 102, 109, 110]. Figure 4.2 shows a sequence of snapshots, during forced stretching, of one independent SMD simulation for poly(A-T)$_{15}$ DNA. The DNA is seen to undergo a series of conformational changes starting from helical form, i.e., B-DNA (marked A in Figure 4.2) and gradually unwinding itself into planar zipper form, i.e., zip-DNA (marked E in Figure 4.2). During the A to E transition the hydrogen bonds between complementary base pairs break; the base pairs are seen to interdigitate and finally all stack on top of each other in a zipper like fashion. Also highlighted in Figure 4.2 are two sets of base pairs, P-P' and Q-Q', which are spaced half a pitch apart (5 bp apart) from each other. The length of the entire DNA changed from 52 Å to 103 Å over the course of the simulation. The extension of the DNA as a function of time is shown in Figure 4.3.

Figure 4.4 shows force-extension curves for five independent SMD simulations performed on the poly(A-T)$_{15}$ DNA strand stretched with a constant pulling speed of 1 Å/ns. At the initial stage, the B-DNA undergoes an elastic transformation, where the force increases gradually from 0 to 100 pN accompanied by a molecular extension of 10 Å. Beyond this extension the force-extension curve is characterized by a plateau region, where the DNA transforms cooperatively from the helical conformation, i.e., B-DNA to a zipper-like form, i.e., zip-DNA. The transition is characterized by coexistence of helical, stretched and zipper DNA domains. During the initial stages of the transition, a zip-DNA nucleation site appears near the pulling end of the DNA whereas the restrained end retains its helicity. Gradually, the DNA extends and unwinds, with parts of the DNA (middle portion) acquiring a stretched conformation (S-DNA), where the complementary base pairs partially unwind but are still bound through hydrogen bonds. Eventually the S-DNA and B-DNA domains transform into zip-DNA domains and at an extension of 38 Å the entire DNA transforms into zip-DNA (see inset in Figure 4.4). The zip-DNA extends elastically beyond 38 Å and is marked

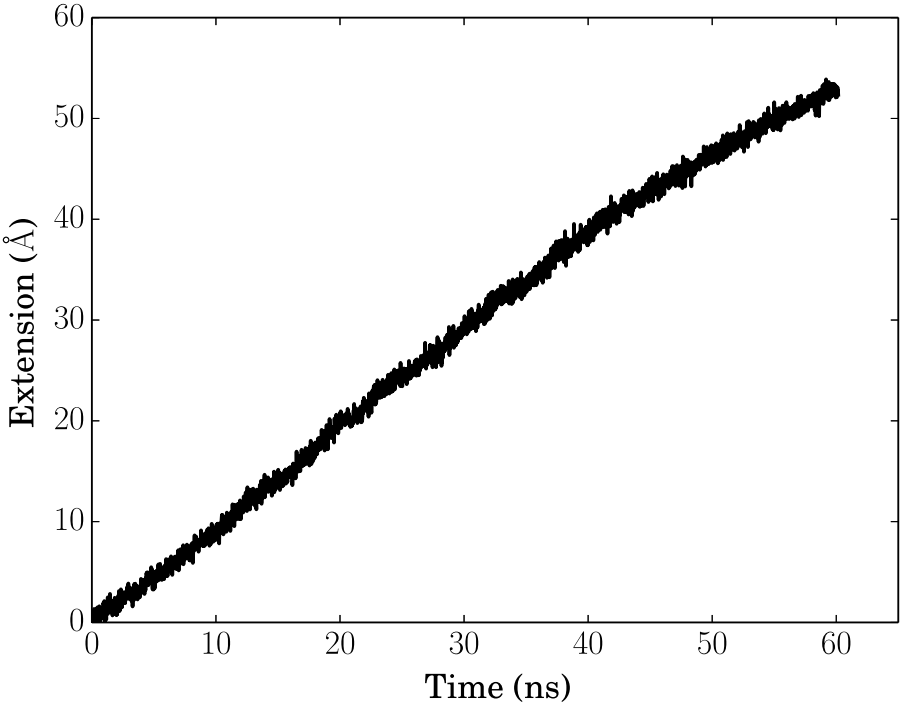

Figure 4.3: Molecular extension of poly(A-T)$_{15}$ DNA over the course of a 60-ns SMD simulation performed at a constant pulling speed of 1 Å/ns.

by a steep increase in the force experienced by the DNA. The computed peak force (1 nN) experienced by the DNA is much higher than the experimental ones ($\approx$ 150 pN) [85, 86, 87]. The discrepancy is attributed to the pulling speeds employed in simulations (1 Å/ns) which, due to limited computational resources, is much larger than the typical pulling speeds in experiments (1 Å/μs).

The evolution of the angle between base pairs P-P' and Q-Q' (see Figure 4.2), for the poly(A-T)$_{15}$ case is shown in Figure 4.5. The two base pairs are a half-pitch apart and the angle is initially, when the DNA assumes a helical form, -180°. After the transition to zip-DNA the base pairs are vertically stacked on top of each other, reducing the angle between the base pairs to 0°. The change in the angle (from -180° to 0°) occurs over a short range of extension, ranging from 10 Å to 25 Å. However, there is a significant variation in the observed dynamics across the five independent simulations.

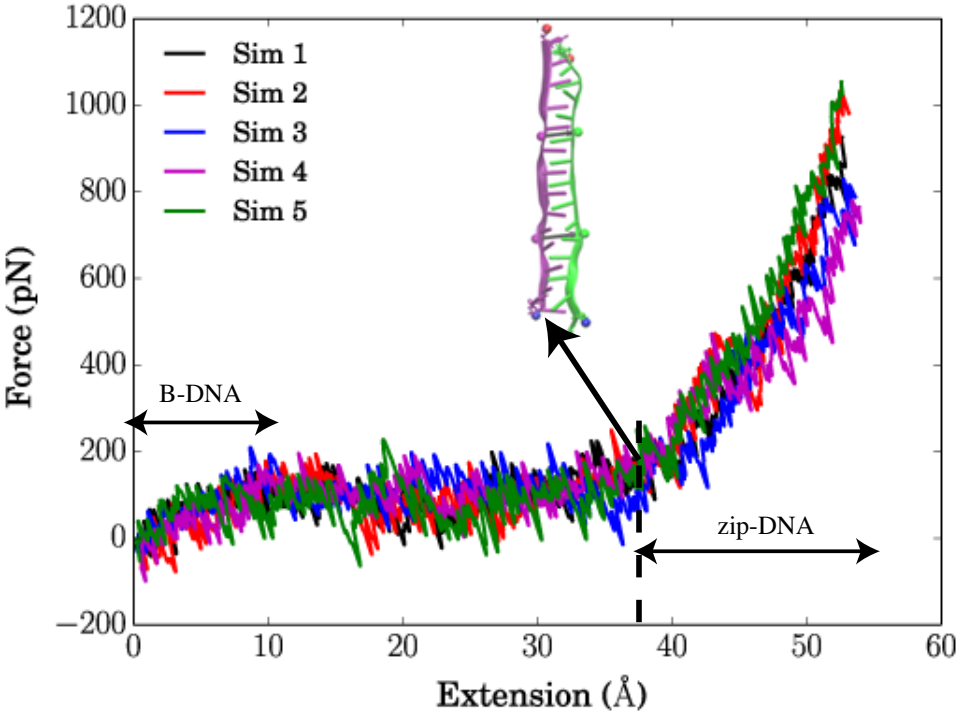

Figure 4.4: Force-extension curves for poly(A-T)$_{15}$ DNA. Shown are the force-extension curves that resulted from five independent SMD simulations, Sim 1-5, performed at a pulling speed of 1 Å/ns. The force-extension curve begins with a region corresponding to the elastic extension of B-DNA followed by a B-DNA to zip-DNA transition plateau. In the region beyond the plateau the zip-DNA undergoes elastic extension, which is characterized by a sharp linear increase in force. The inset shows the zip-DNA conformation at the end of the transition plateau.

This variation can be attributed to fast pulling employed in the simulation, which does not allow dsDNA's slower degrees of freedom to relax completely during the simulation time covered (60 ns).

4.4 DNA conformation detection using transverse electronic conductance

Charge distributions corresponding to DNA conformations at five intermediate steps of the B-DNA to zip-DNA transition, A through E in Figure 4.2,

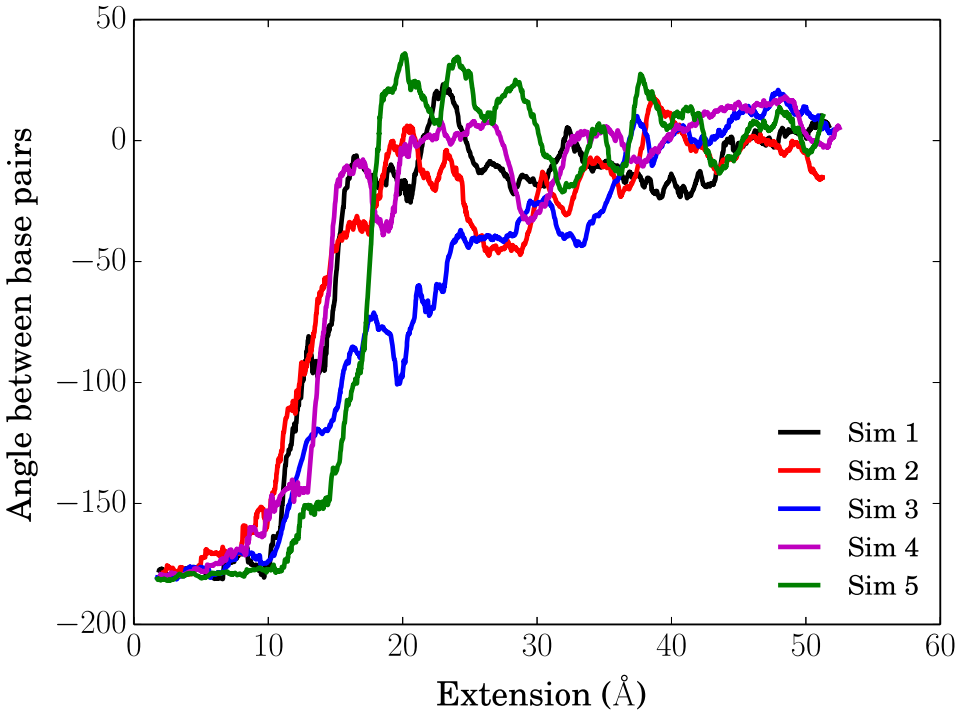

Figure 4.5: Evolution of the angle between base pairs P-P' and Q-Q' (see Figure 4.2) for five independent SMD simulations, Sim 1-5, performed on poly(A-T)$_{15}$ DNA; the angle changes from -180° to 0° as the DNA segment between P-P' and Q-Q' transitions from helical to zipper form.

were extracted from the all-atom MD trajectory. The DNA charge distribution, for each of the intermediate stages, was then placed inside a graphene nanopore with a diameter = 2.4 nm, such that the base pair P-P' resides inside the graphene nanopore; in addition, the DNA axis was also aligned with the nanopore axis. These charge distributions were then "translocated" along the -z direction in steps of 0.5 Å, until the base pairs Q-Q' reached the pore. At each step the electrostatic potential induced by the DNA on the graphene nanopore was calculated using the Poisson-Boltzmann approach. The electrostatic potential maps, in the plane of the graphene membrane, altered step-by-step due to DNA translocation, are provided for both B-DNA and zip-DNA cases in Figures 4.6 and 4.7.

The electrostatic potentials determined according to Eq. 5.1 were then included in the Hamiltonian of the graphene membrane (see Eq. 4.3) to calculate the resulting conductance across the graphene membrane by means of

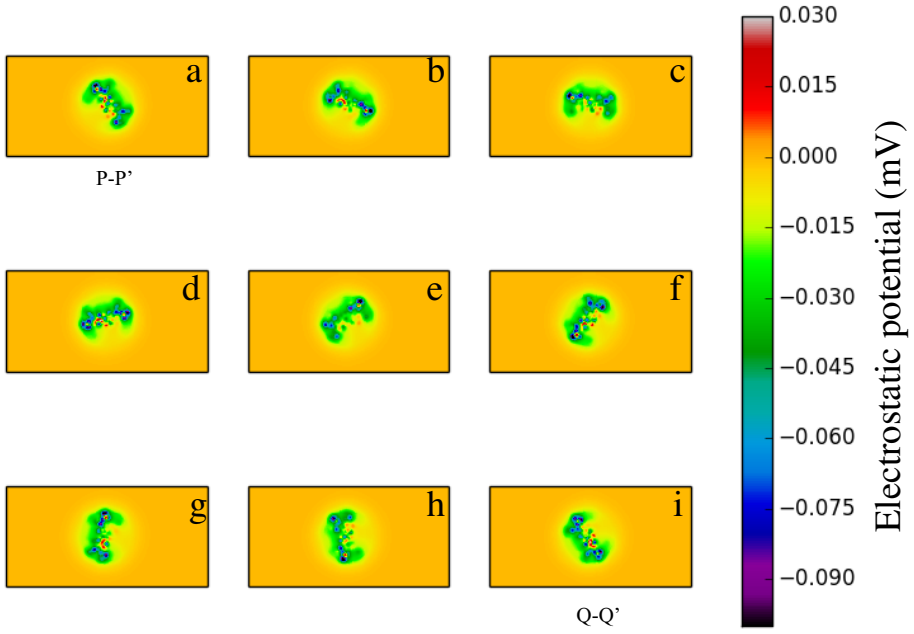

Figure 4.6: Snapshots of the electrostatic potential profile of B-DNA in the graphene membrane at 1 M KCl concentration. The electrostatic potential profiles (a-i) correspond to translocation of the DNA segment, comprising of base pairs between P-P' and Q-Q', through the nanopore. The B-DNA, due to the helical DNA conformation, rotates by 180° in the plane of the graphene membrane. Along with the DNA rotation the electrical field also rotates inside the graphene nanopore, which induces oscillations in the transverse electronic conductance.

Eq. 5.3 and as further outlined in Section 4.2. Shown in Figure 4.8 is the transverse conductance as a function of DNA position inside the nanopore. The DNA inside the graphene nanopore was assumed to be stretched and for this purpose the different intermediate stages (A-E) during the B-DNA to zip-DNA transformation obtained from a SMD simulation performed on poly(A-T)$_{15}$ were adopted. The calculations described were carried out for two graphene nanopore geometries: an armchair edge geometry with width of 5 nm, and a quantum point contact (QPC) edge with width of 8 nm. The QPC edge has an irregular edge shape, leading to more stringent boundary conditions for electron transport when compared to the flat armchair edge geometry [111]. (The exact lattice of the armchair and QPC edge are provided in Figure 4.9). As one can see in Figure 4.8, the conductance varies

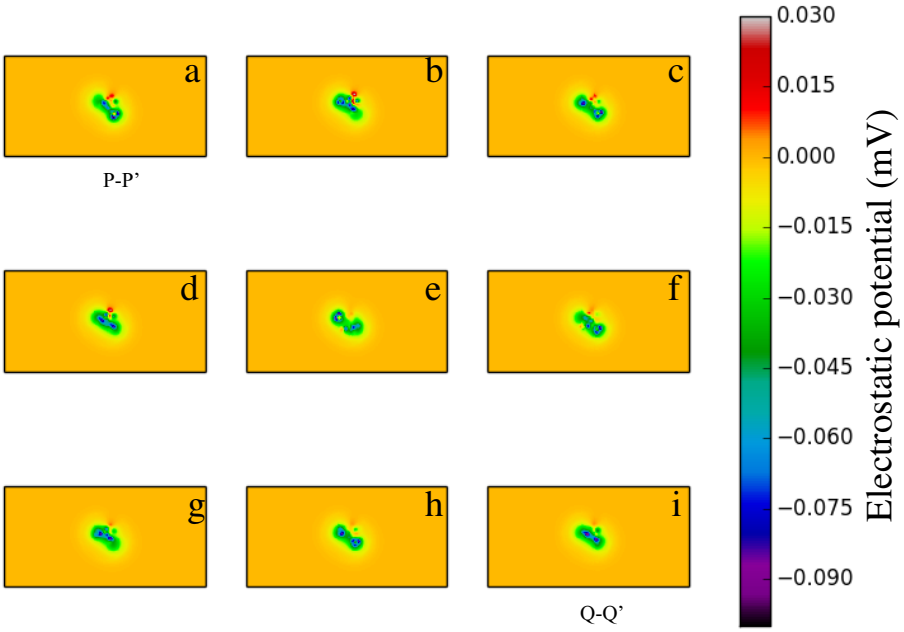

Figure 4.7: Snapshots of the electrostatic potential profile of zip-DNA in the graphene membrane at 1 M KCl concentration. The electrostatic potential profiles (a-i) correspond to translocation of the DNA segment, comprising of base pairs between P-P' and Q-Q', through the nanopore. The zip-DNA, due to the linear DNA conformation, does not rotate in the plane of the graphene membrane leading to a constant transverse electronic conductance.

sinusoidally for stage A DNA translocating through the nanopore, is constant for stage E DNA translocating, and adopts an intermediate variation for stage B, C, D DNA translocating.

Translocation of the DNA segment, comprising of nucleotides between P-P' and Q-Q', in the helical form results in an apparent rotation of the surrounding electric field inside the nanopore (see Figure 4.6). As a result, the transverse electronic conductance in the graphene membrane being induced by the field oscillates. In case of zip-DNA being translocated through the pore the field is rotationally invariant and, as a result, the transverse conductance remains constant (see Figure 4.7). In case of progressive extension of the DNA accompanied during a B-DNA to zip-DNA transition the

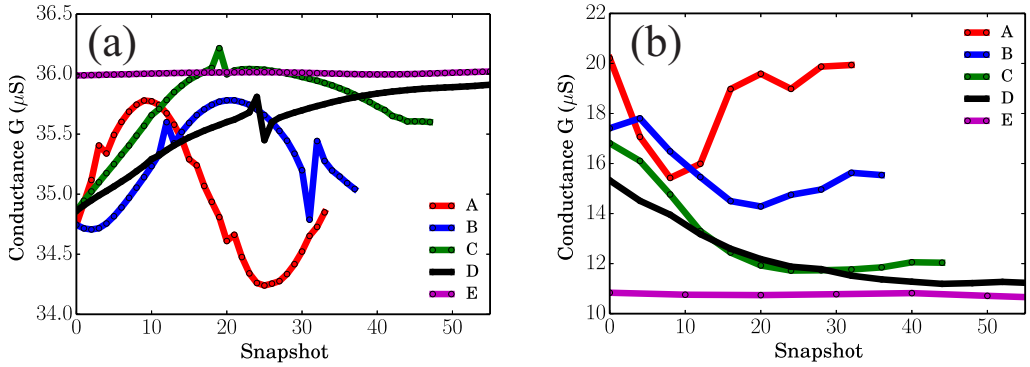

Figure 4.8: Transverse electronic conductance as a function of poly(A-T)$_{15}$ DNA position (snapshot) for (a) graphene nanopore with armchair edge, and (b) graphene nanopore with QPC edge. base pairs P-P' were initially aligned with the nanopore, and subsequently translocated at a rate of 0.5 Å, along -z direction, per snapshot until base pairs Q-Q' reached the pore. The transverse electronic conductance changes from an oscillating type response, corresponding to B-DNA (A), to a constant conductance when the DNA adopts a zipper-like conformation, i.e., zip-DNA (E). Sinusoidal variation in the transverse electronic conductance diminishes as the DNA passes through the intermediate stages B,C, and D. A QPC edge geometry shows larger variations in transverse electronic conductance when compared to the armchair edge geometry.

sinusoidal variation of the transverse conductance diminishes as the translocating DNA passes through the A, B, C, D, and E stages shown in Figure 4.2. Translocation of the DNA segment, comprised of base pairs between P-P and Q-Q', is equivalent to a rotation, in the plane of the graphene nanopore, by an amount equal to the angle between the base pairs P-P' and Q-Q' (see Figure 4.5). Thus, the conductance variation is a measure of the helicity of the DNA and can be used to detect the DNA conformation. The total variation in conductance for the B-DNA is about 1.5 μS for the arm chair edge (G(max)-G(min)+G(max)-G(0)) and about 10 μS for the QPC edge (G(max)-G(min)+G(0)-G(min)). The conductance variation is enhanced for the QPC edge case due to the constriction, which affects the electron transport near the nanopore. In addition, the boundaries also influence the shape of the response which no longer looks perfectly sinusoidal in case of a QPC edge pore.

The conductance variation as a function of DNA extension is shown in

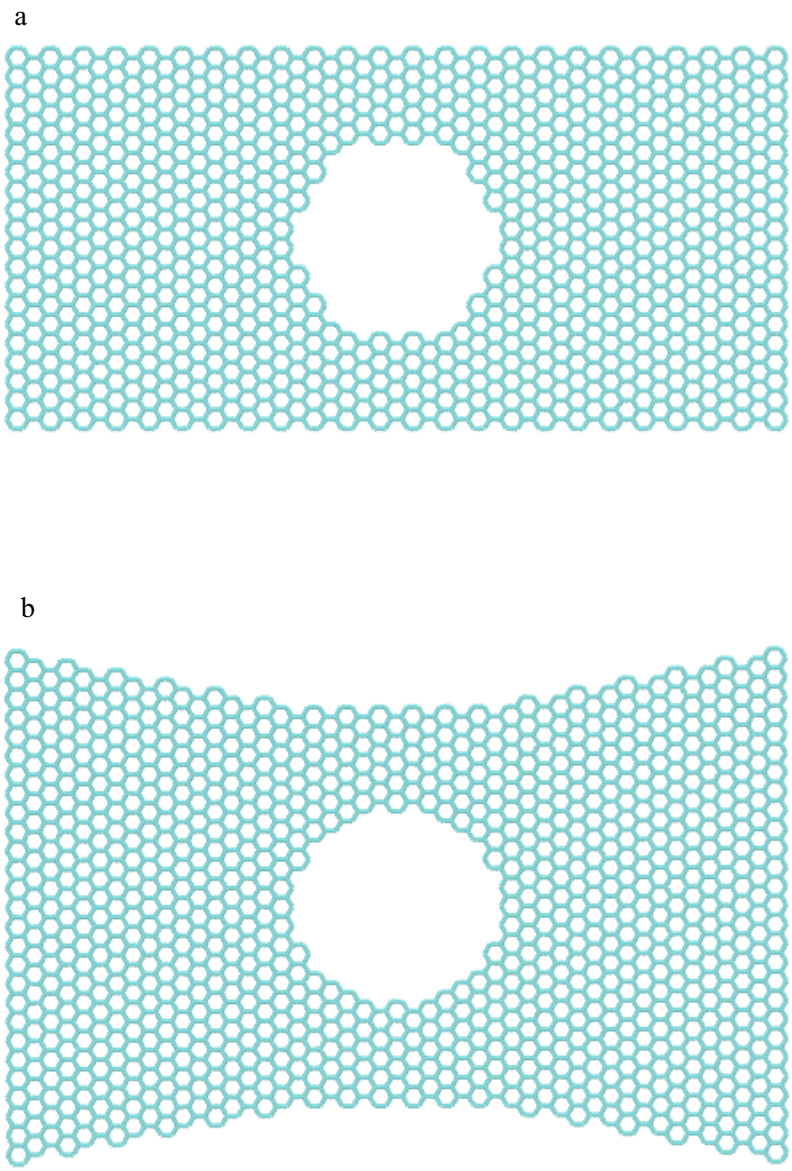

Figure 4.9: The graphene lattices, with pore diameter = 2.4 nm, employed in the calculation of transverse electronic conductance: (a) 5 nm-wide armchair edge nanoribbon and (b) 8 nm-wide QPC edge nanoribbon.

Figure 4.10 for poly(A-T)$_{15}$ and poly(G-C)$_{15}$ strands computed at two different KCl molar concentrations, namely, 1 M (Figure 4.10a) and 0.1 M (Figure 4.10b). The error bars were obtained from sampling over five independent simulation trajectories for both poly(A-T)$_{15}$ and poly(G-C)$_{15}$. The

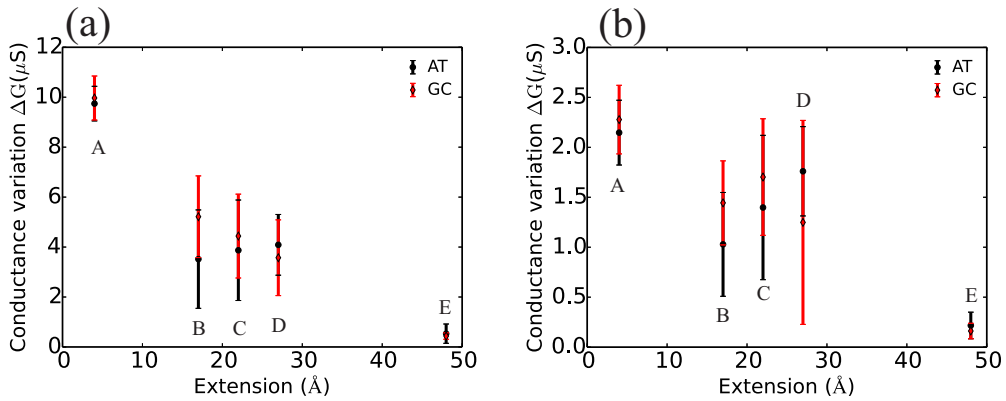

Figure 4.10: Variation in the transverse electronic conductance as a function of DNA extension for a QPC edge graphene nanopore. Shown in (a) and (b) are conductance variation, for the stages A, B, C, D, and E (see Figure 4.2) arising in the B-DNA to zip-DNA transition corresponding to KCl molar concentrations of 1 M and 0.1 M respectively. The error bars are obtained from sampling over five independent force-extension simulations performed on poly(A-T)$_{15}$ and poly(G-C)$_{15}$ strands.

QPC edge, because of its higher sensitivity compared to the armchair edge, was employed in the conductance calculations presented in Figure 4.10. For both high and low molarity cases, the conductance variation decreases as the DNA transitions from B-DNA to zip-DNA. The uncertainty in the conductance variation is significantly larger for the intermediate stages B, C, and D as compared to stages A (helical) and E (zipper), which can be attributed to the broader distribution in the unwinding pathways sampled by the independent MD simulations.

As discussed above, the conductance variation is a measure of the helicity and there is a large heterogeneity in the helical angle, between P-P' and Q-Q' (see Figure 4.5), observed in regions, where DNA transitions from B-DNA to zip-DNA. In the present study, limited though by small sampling, conductance variations are indistinguishable for poly(A-T)$_{15}$ and poly(G-C)$_{15}$ cases. The general trend in conductance does not change when the molarity is changed from 1 M to 0.1 M. However, the magnitude of conductance variations is suppressed for the low molarity case, e.g., conductance variation for B-DNA (A in Figure 4.10) reduces from 10 μS to 2 μS for a change in molar concentration from 1 M to 0.1 M. In the low molarity case, due to reduced screening, the average potential induced on the graphene membrane is much

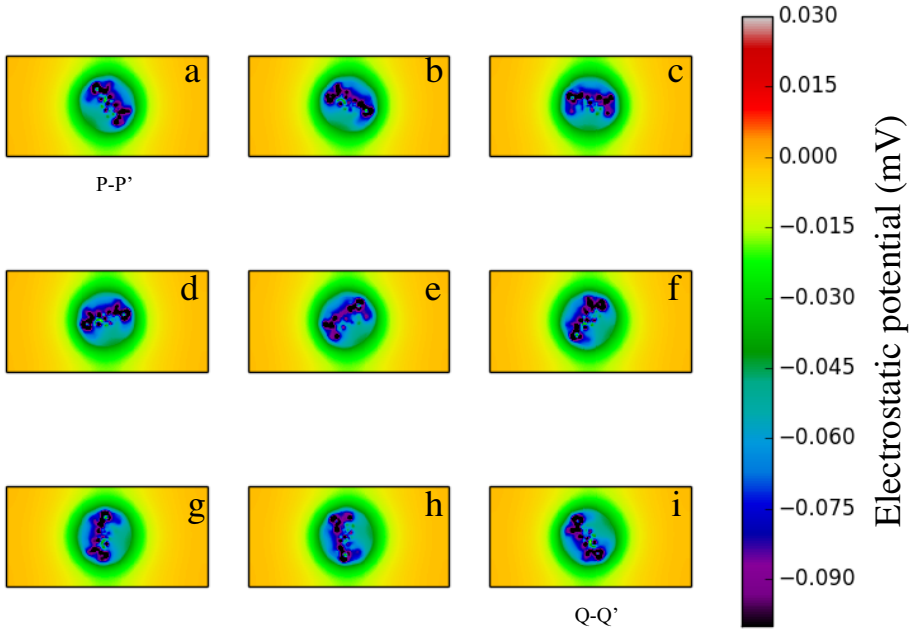

Figure 4.11: Snapshots of the electrostatic potential profile of B-DNA in the graphene membrane at 0.1 M KCl concentration. The electrostatic potential profiles (a-i) correspond to translocation of the DNA segment, comprising of base pairs between P-P' and Q-Q', through the nanopore. Due to reduced screening the electrostatic potential profile has a slower spatial decay when compared to the 1 M case (see Figure 4.6).

larger in magnitude compared to the high molarity case (see Figures 4.11 and 4.12), which is equivalent to a gating effect and changes the bias point of the QPC significantly [100]. Although reduced screening, at low molar concentrations, increases the magnitude of the potential induced at the pore mouth, the variation in conductance itself is not enhanced.

4.5 Conclusion

In summary, we propose a novel detection technique to sense dsDNA in different structural conformations (helical and zipper) by means of transverse electronic conductance in graphene nanopores. The oscillations in trans-

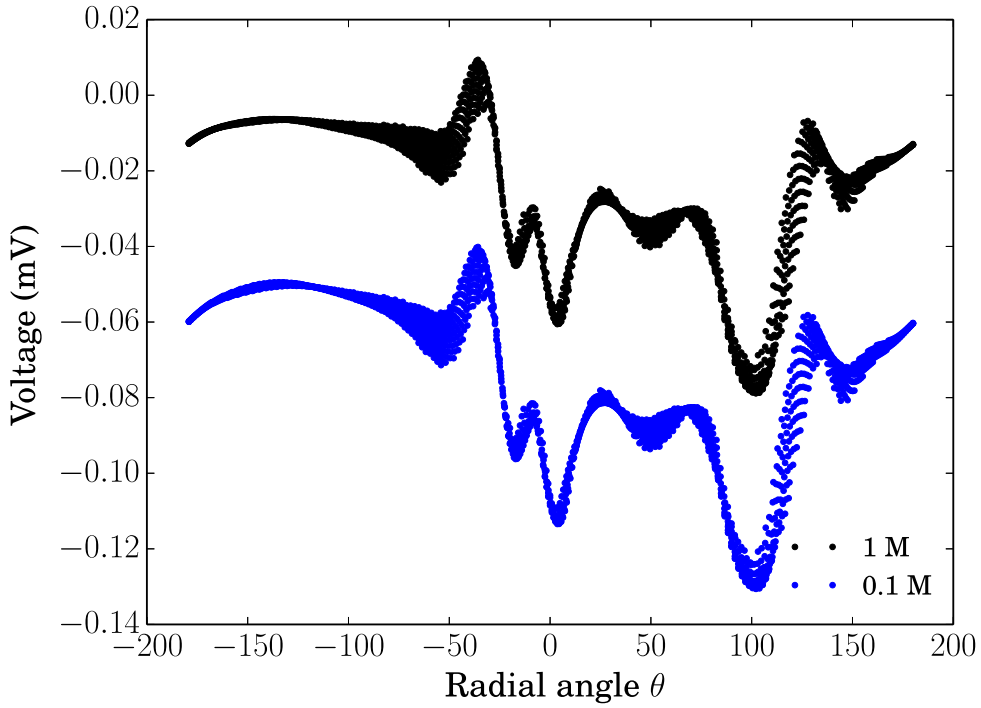

Figure 4.12: Radial distribution of electrostatic potential at the nanopore edge under KCl molar concentrations of 1 M and 0.1 M. The potentials correspond to a DNA conformation, where the base pair P-P' is inside the nanopore. At low molarity the potential in the vicinity of the pore is much larger (in magnitude) than 1 M case due to reduced screening.

verse electronic conductance arising due to the helical nature of the B-DNA vanish when B-DNA undergoes a structural transition to zip-DNA. Probing the structure of DNA using the transverse electronic conductance through graphene membranes can be a useful tool in the rapidly evolving field of DNA nanosensors. The computational approach used in the present study combines data from extensive classical mechanical all-atom molecular dynamics simulations (0.6 μs in total) to describe intermediate conformations of dsDNA and from quantum mechanical NEGF-based calculations of transverse electronic conductance in graphene membranes: the two calculations are coupled through embedding the DNA charge distribution resulting from the MD simulation into a Poisson-Boltzmann description of the electrostatic potential in a physiological KCl solution and adding the resulting potential to the quantum mechanical calculation of the graphene sheet current. The re-

sults suggest the capability of graphene nanopores to detect conformational changes of dsDNA through measurement of the transverse electronic conductance (sheet current). Such measurement can supplement ionic blockade currents to assess the local conformation of translocating DNA in nanopore sensors. Observed trends in the membrane conductance for dsDNA are predominantly a signature of the backbone, which screens out the response due to the base pairs, making it difficult to observe any sequence dependent (AT/GC) changes.

CHAPTER 5

DETECTING SSDNA TRANSLOCATION AT SINGLE BASE PAIR RESOLUTION

5.1 Introduction

In the present chapter we show the ability of graphene nanopores to distinctively count base pairs in an ssDNA molecule translocating through graphene nanopore. Our study shows that the position of the pore can drastically enhance the shape of the conductance signals, an off-center pore seems to have a sharper response to translocating base pairs. Further, we show that diameter and shape of the pore play a significant role in the sensitivity of calculated conductance signal.

5.2 Methods

Steered molecular dynamics simulations (SMD) were employed to stretch a 16-bp-ssDNA, comprising of four repetitions of the DNA segment A-T-G-C, from a canonical helical conformation to a linear, ladder-like form. The ssDNA molecule was solvated in a 0.3 M KCl electrolyte solution, and the 5' end of the ssDNA was pulled with a constant velocity of 10 Å/ns, while the 3' end of the DNA was harmonically constrained to its initial position, until the nucleotides in the central region of the ssDNA acquired a linear conformation. The molecular extension of the ssDNA changed from 55 Å to 128 Å over the course of the simulation, and the base pairs collectively tilted toward the 5' end of the DNA [6]. The program NAMD [49] was used to perform the molecular dynamics simulations with CHARMM27 [51] force-field parameters to model ssDNA, K^+ and Cl^- ions, and TIP3P model to treat water molecules. The electrostatic potential induced by the ssDNA charge distribution, inside a nanopore within a GNR, was modeled using a

self-consistent Poisson equation [3]

$$\nabla \cdot [\epsilon(\vec{r})\nabla\phi(\vec{r})] = -e[K^+(\vec{r},\phi) - Cl^-(\vec{r},\phi)] - \rho_{DNA}(\vec{r}) \tag{5.1}$$

where $\phi(\vec{r})$ is the electrostatic potential, $\epsilon(\vec{r})$ is the local permittivity, and $\rho_{DNA}(\vec{r})$ is the three-dimensional charge distribution due to the DNA molecule. The electrolytic ions in solution are distributed according to a Boltzmann distribution

$$K^+(\vec{r},\phi) = c_0 \exp(-e\phi/k_{\mathrm{B}}T), \quad Cl^-(\vec{r},\phi) = c_0 \exp(e\phi/k_{\mathrm{B}}T) \tag{5.2}$$

Here, $K^+(\vec{r})$ and $Cl^-(\vec{r})$ are the spatial ion concentrations, e is the electronic charge and c_0 is the molarity of the KCl solution (0.3 M). The electrostatic potential induced by the ssDNA on the graphene membrane modulates the transmission function ($\bar{T}(E)$) of the graphene nanoribbon, calculated using the non-equilibrium Green's function (NEGF) technique as outlined elsewhere in detail [82, 100]. The conductance across the GNR at a particular bias V_{DS} is given by [82, 100]

$$G = \frac{2e}{V_{DS}h} \int_{-\infty}^{\infty} \bar{T}(E)[f_1(E) - f_2(E)]dE \tag{5.3}$$

where $f_\alpha(E) = f(E - \mu_\alpha)$ is the probability that an electron occupies a state at energy E in the lead α, $\mu_1 - \mu_2 = V_{DS}$ is the bias across the conductor. μ_1, which is chosen to be equal to 0.0 eV with respect to the tight binding parameters taken from [81], lies in the valence band. We choose to bias the leads to this value, because, here, the g-QPC conductance is maximally sensitive to external charges. In our calculations we assumed $f(E)$ to be the Fermi-Dirac distribution, $V_{DS} = 5$ mV and a system temperature of 295 K was adopted.

5.3 Results and discussion

The stretched ssDNA, which adopts a ladder-like configuration due to forced extension, was placed inside a nanopore within a quantum point contact (QPC)-edged graphene nanoribbon (g-QPC) and translocated at a rate of

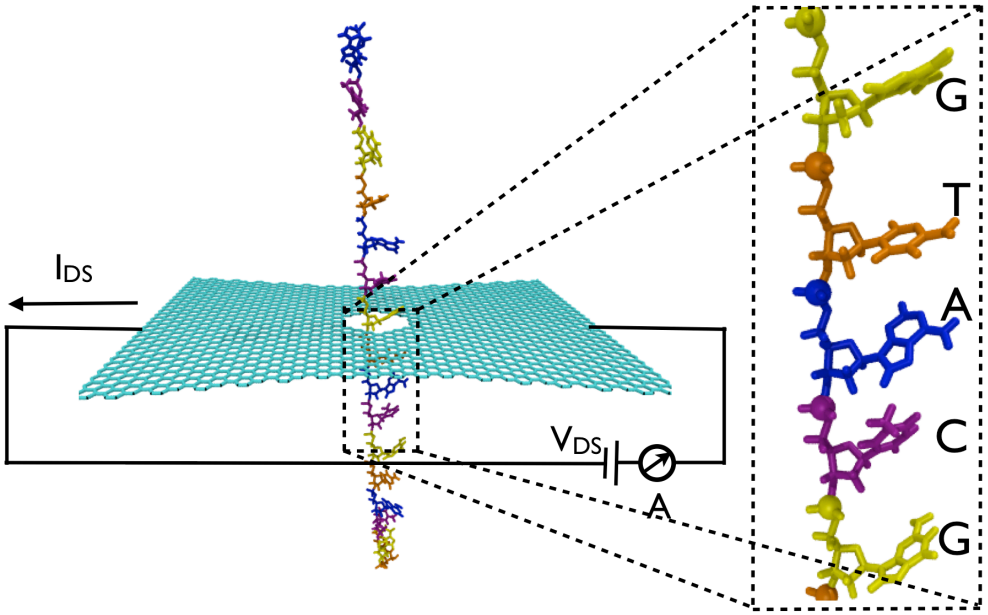

Figure 5.1: Schematic of the graphene nanopore system used to calculate transverse electronic conductance. Shown in the figure is the ssDNA conformation, which arose from a MD simulation of forced extension of ssDNA. The extended ssDNA was placed inside a QPC edge graphene nanoribbon (g-QPC) and translocated at a rate of 1 Å per snapshot. Transverse electronic conductance was computed for the five base pairs shown in the inset of the figure.

1 Å per snapshot, along a direction perpendicular to the graphene plane, to mimic electrophoretic translocation of the DNA through the graphene nanopore (see Figure 5.1). A g-QPC with a width of 8 nm and pinch of 5 nm was employed in current study. The reason for employing QPC edge is discussed elsewhere [111], where we have also shown that the rotation of the electrical potential of the DNA charge distribution, arising from DNA helicity, within the graphene plane causes a modulation in the electronic conductance through the graphene membrane. In the present study, we choose a ladder-like conformation for ssDNA to ensure that the conductance modulations are solely due to the linear translocation of the DNA as opposed to any effective rotation of the electrostatic potential in the graphene plane.

The transverse electronic conductance of the g-QPC as a function of the

ssDNA snapshot, translocating through a circular nanopore with a 1.2 nm diameter, is shown in Figure 5.2. We study the ssDNA translocation through such a nanopore at three different locations. Figure 5.2a corresponds to the center of the nanopore aligned to the geometric center of the g-QPC. In Figure 5.2b and Figure 5.2c the nanopore center is offset from the geometric center by 1 nm and 2 nm respectively along the y-direction defined in Figure 5.2. In each of the three cases, we choose to study two orientations of the DNA molecule one where the base pairs are aligned in the direction of transverse electronic current, herein referred to as ssDNA-x (see Figure 5.2d) and where the base pairs are aligned in direction perpendicular to the transverse electronic currents herein referred to as ssDNA-y (see Figure 5.2e).

For both DNA orientations, the conductance displays a series of peaks and valleys corresponding to the passage of individual nucleotides, which are attached to the negatively charged phosphate backbone, across the graphene membrane. The variation in electrical potential on the nanopore edge due to the motion of charges on the DNA molecule during the translocation process varies the local Fermi energy in the graphene membrane, altering the conductance [111].

The particular snapshot when a nucleotide's center of mass passes the graphene membrane is denoted with a dashed line in Figure 5.2. As can be readily seen, these snapshot locations correlate with the valleys in the conductance curve, identifying a conductance valley with the passage of a single nucleotide. The magnitude of the conductance at a particular snapshot is determined by the spatial orientation of the nucleotide within the nanopore, which can fluctuate significantly. However, the percentage change in conductance between nucleotides can be in excess of 15%, indicating that one can distinguish the charges of a passing nucleotide from the rest of the system.

In particular, the magnitude of the conductance variations for ssDNA-y is $0.03\ \mu$S to $0.05\ \mu$S, or 10 to 17% of the overall signal. These variations are approximately three times larger than those of ssDNA-x. This due to the fact that for this particular nanopore and QPC edge geometry, there is a larger electronic density of states above and below the nanopore (along the y-direction) compared to the density of states on the either side (x-direction).

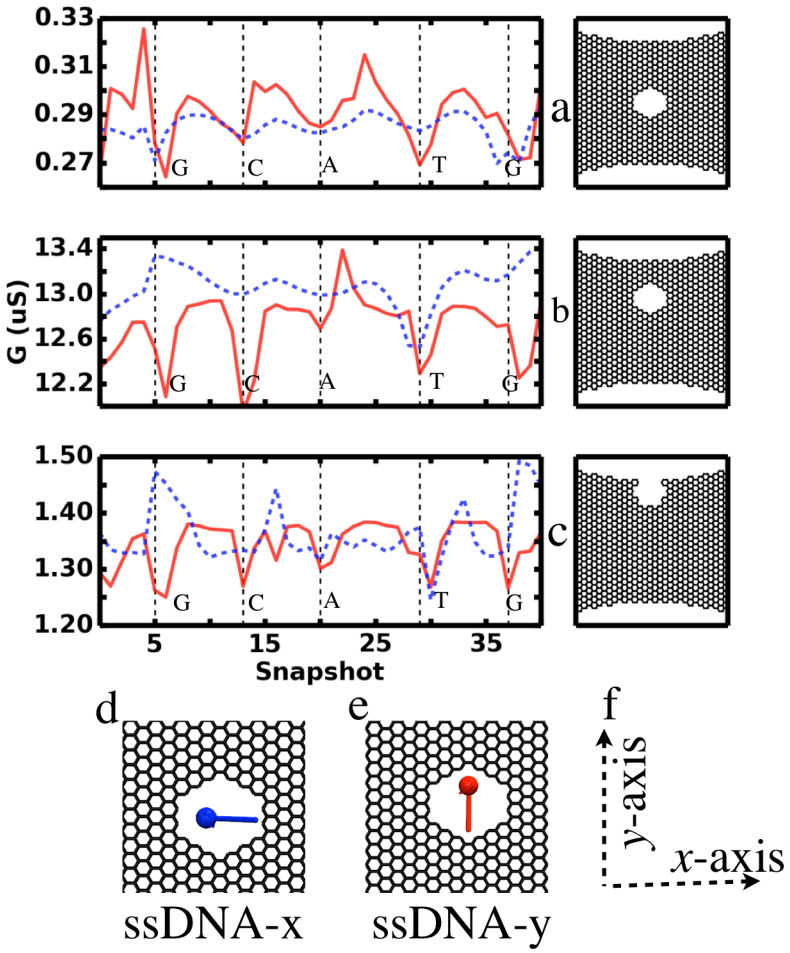

Figure 5.2: Transverse electronic conductance, as a function of DNA position (snapshot), arising in a QPC-edged graphene membrane due to translocation of five base pairs of an ssDNA molecule in a linear ladder-like conformation (see inset Figure 5.1). The dips in the conductance correspond to the translocation of a single base pair through the nanopore. Three different nanopore geometries are investigated (a) nanopore center is aligned to the geometric center of the graphene membrane, (b) nanopore center is offset by 1 nm from the geometric center, and (c) nanopore center is offset by 2 nm from the geometric center. For each of the geometries the base pairs were translocated in two different configurations: (d) ssDNA-x, where the base pairs are aligned in the direction of transverse electronic current and (e) ssDNA-y where the base pairs are aligned in direction perpendicular to the transverse electronic currents. The coordinate axis is shown in (f).

This is because the nucleotides of ssDNA-y are closer to the larger electron density compared to ssDNA-x. As a result, changes in electrical potential

have a more significant affect on the conductance.

In order to determine how altering the pore position can affect the conductance sensitivity, we chose to study g-QPCs with a 1.2 nm diameter pore in two alternate positions, shown in Figures 5.2b and c. When the pore geometry is altered, such as when changing its position, shape, or size, the boundary conditions restricting the allowed electronic states in the QPC are likewise changed. This forces various conduction channels around the Fermi energy to open or close, and depending on the transmission probability of each of these channels, an overall larger or smaller current can arise. An in-depth discussion on the effects of geometry on the electronic states and electronic transmission is elaborated in [111].

Because the trajectory of ssDNA remains unchanged for each pore position, the conductance of the QPC with a pore at position "b" (Figure 5.2b) has conductance minima at the same nucleotide positions as that with the pore at "a". However, for ssDNA-y, the width of these variations is noticibly smaller. Similarly, the width of the minima is further reduced for a QPC with a pore at position "c" (Figure 5.2c) for ssDNA-y. This is due to the fact that there is a smaller interaction between the charges on the DNA backbone and the electronic conduction states. These backbone charges, which are negatively charged, tend to attract positive holes in the g-QPC, enhancing the hole conduction and can significantly mask the nucleotide signal. As the nanopore is placed closer to the edge, however, the influence of the backbone becomes negligible, especially when outside of the conductor, as in the case of pore "c". As a result, the nucleotide charges are solely responsible for the conductance variation, enhancing the detection of the nucleotide passage event.

In the case of the ssDNA-x, as the pore is placed closer to the edge, the nucleotide signal becomes indiscernible. The main reason being, in this orientation, there is little interaction between the nucleotide and the conducting holes when placed far from the QPC center, whereas in the ssDNA-y orientation nucleotides are adjacent to the conduction charges.

The most striking effect of the differing boundary conditions due to vary-

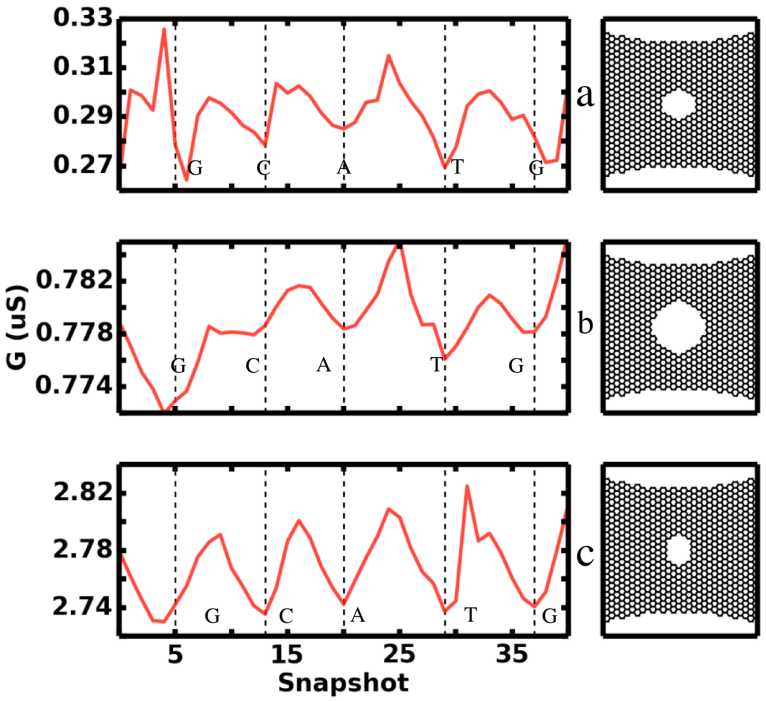

Figure 5.3: Influence of pore size and shape on electronic conductance due to translocation of five base pair long ssDNA segment in a linear ladder-like conformation. Shown in the figure are conductance for the cases (a) circular pore with diameter = 1.2 nm, (b) circular pore with diameter = 2 nm, and (c) elliptical pore with major and minor axis diameters equal to 1.2 nm and 0.8 nm respectively.

ing pore position is their influence on the conductance magnitude. When the pore is moved from position "a" to position "b", the conductance is magnified by almost two orders of magnitude, and at position "c", the conductance is further reduced by a factor of 10. Such drastic changes in the conductance magnitude with alternate pore positions suggests that the conductance magnitude is a strong function of lattice geometry. However, finer control of the conductance magnitude can be achieved by adjusting the Fermi energy of the g-QPC via a gate electrode [100]. It is clear that positioning the pore closer to the boundary negates the influence of the phosphate backbone on the conductance, and hence increases the ability for the current to detect only the nucleotide.

In Figure 5.3 we see the conductance, due to ssDNA-y, for a 2 nm pore and a 0.8 nm by 1.2 nm elliptical pore at the g-QPC center in addition to

the 1.2 nm pore discussed earlier. The primary result of increasing the pore diameter to 2 nm is the suppression of the interaction between the ssDNA molecule and the electronic conduction states. Since the ssDNA is in the center of the pore, the electrolytic screening, with a Debye length of 0.5 nm, causes the electric potential to become significantly smaller at the pore edge. Variations can still be seen at the same locations as the 1.2 nm pore, but they are significantly smaller, varying in magnitude by 1%.

One of the main issues encountered when electrically sensing a DNA molecule, translocating through a nanopore, is the stochastic fluctuations of the DNA molecule itself reducing or eliminating the conductance variations due to the passage of a nucleotide. Employing an elliptical pore can restrict the lateral fluctuations of translocating base pair and we investigate the conductance due to ssDNA-y translocating in an elliptical pore with a major and minor axis diameter equal to 1.2 nm and 0.8 nm respectively. The conductance variations become much more uniform and well defined when the ssDNA-y is translocating through the elliptical pore. This is because the potential on the pore edge is screened less by the electrolyte since the edge is closer to the DNA charges of which the contribution due to phosphate backbone dominates. As a result, the conductance signal is more of the passage of the phosphate atoms than the nucleotides themselves. The conductance variations are still significant, having a magnitude 3% of the overall conductance.

5.4 Conclusion

In conclusion, we show it is possible to discretely count individual base pairs of an ssDNA molecule using transverse electronic conductance in a quantum point contact graphene nanoribbon with a nanopore. The orientation of the DNA within the nanopore and the position of the nanopore itself determines the strength of the interaction between the nucleotides and the electron density, affecting the fidelity of the signal. Moving the pore closer to the edge reduces the influence of the phosphate backbone when the ssDNA is oriented inward, enhancing the detection of passing nucleotides. Larger pores make nucleotide detection difficult, so achieving a small pore diameter is crucial

for maximum sensing ability. In addition, the behavior of the conductance response is a function of nanopore shape, perhaps implying that more precise engineering of nanopore geometry can allow for stronger detection events.

CHAPTER 6

SUMMARY

This dissertation has explored some aspects of DNA sensing using graphene nanopores by employing classical molecular dynamics simulations and quantum mechanical non-equilibrium Green's function (NEGF)-based transport simulations. The work presented in this thesis was the first molecular dynamics (MD) study of electrophoresis of DNA through graphene nanopores. We demonstrated that MD simulations yield ionic current blockade characteristics consistent with experiments and suggested the ability to discern A-T and G-C base pairs under suitable conditions. MD simulations can thus guide the design of graphene-based sensors for DNA sequencing applications.

Electronic sheet current measurements in graphene membranes provides an alternate means to probe translocating base pairs through nanopore sensors. We demonstrated the ability of graphene nanoribbons to detect the rotational and positional conformation of DNA inside the nanopore using a self-consistent Poisson Boltzmann formalism coupled to NEGF-based transport simulations.

The sensitivity of the sheet current depends critically on an orderly passage of DNA and optimal sensitivity can arise when the passing DNA is stretched mechanically. We show electronic detection, via sheet currents, of conformational transition of dsDNA from helical to zipper-like form. Probing such structural transitions of DNA using transverse electronic conductance can be a useful tool in the rapidly evolving field of DNA sensors. The last part of the dissertation shows how mechanically manipulating an ssDNA into a ladder conformation can allow sheet currents to sense translocating ssDNA at single base pair resolution.

REFERENCES

[1] S. Howorka and Z. Siwy, "Nanopore analytics: Sensing of single molecules," *Chem. Soc. Rev.*, vol. 38, no. 8, pp. 2360–2384, 2009.

[2] J. J. Kasianowicz, E. Brandin, D. Branton, and D. W. Deamer, "Characterization of individual polynucleotide molecules using a membrane channel," *Proc. Natl. Acad. Sci. USA*, vol. 93, pp. 13 770–13 773, 1996.

[3] M. E. Gracheva, A. Xiong, A. Aksimentiev, K. Schulten, G. Timp, and J.-P. Leburton, "Simulation of the electric response of DNA translocation through a semiconductor nanopore-capacitor," *Nanotechnology*, vol. 17, pp. 622–633, 2006.

[4] M. Zwolak and M. D. Ventra, "Electronic signature of DNA nucleotides via transverse transport," *Nano Lett.*, vol. 5, pp. 421–424, 2005.

[5] C. Dekker, "Solid-state nanopores," *Nature Nanotech.*, vol. 2, no. 4, pp. 209–215, 2007.

[6] J. Mathé, A. Aksimentiev, D. R. Nelson, K. Schulten, and A. Meller, "Orientation discrimination of single stranded DNA inside the α-hemolysin membrane channel," *Proc. Natl. Acad. Sci. USA*, vol. 102, pp. 12 377–12 382, 2005.

[7] A. J. Storm, J. H. Chen, X. S. Ling, H. W. Zandergen, and C. Dekker, "Fabrication of solid-state nanopore with single-nanometre precision," *Nat. Mater.*, vol. 2, pp. 537–540, 2003.

[8] J. Li, D. Stein, C. McMullan, D. Branton, M. J. Aziz, and J. A. Golovchenko, "Ion-beam sculpting at nanometre length scales," *Nature*, vol. 412, pp. 166–169, 2001.

[9] B. M. Venkatesan, A. B. Shah, J. M. Zuo, and B. R, "DNA sensing using nano-crystalline surface enhanced Al2O3 nanopore sensors," *Adv. Funct. Mater.*, vol. 20, pp. 1266–1275, 2010.

[10] A. Mara, Z. Siwy, C. Trautmann, J. Wan, and F. Kamme, "An asymmetric polymer nanopore for single molecule detection," *Nano Lett.*, vol. 4, pp. 497–501, 2004.

[11] A. J. Storm, J. H. Chen, H. W. Zandbergen, and C. Dekker, "Translocation of double-strand DNA through a silicon oxide nanopore," *Phys. Rev. E*, vol. 71, pp. 051 903–051 913, 2005.

[12] J. B. Heng, C. Ho, T. Kim, R. Timp, A. Aksimentiev, Y. V. Grinkova, S. Sligar, K. Schulten, and G. Timp, "Sizing DNA using a nanometer-diameter pore," *Biophys. J.*, vol. 87, pp. 2905–2911, 2004.

[13] J. B. Heng, A. Aksimentiev, C. Ho, P. Marks, Y. V. Grinkova, S. Sligar, K. Schulten, and G. Timp, "Stretching DNA using an electric field in a synthetic nanopore," *Nano Lett.*, vol. 5, pp. 1883–1888, 2005.

[14] J. B. Heng, A. Aksimentiev, C. Ho, P. Marks, Y. V. Grinkova, S. Sligar, K. Schulten, and G. Timp, "The electromechanics of DNA in a synthetic nanopore," *Biophys. J.*, vol. 90, pp. 1098–1106, 2006.

[15] Q. Zhao, J. Comer, S. Yemenicioglu, A. Aksimentiev, and G. Timp, "Stretching and unzipping nucleic acid hairpins using a synthetic nanopore," *Nucleic Acids Res.*, vol. 36, pp. 1532–1541, 2008.

[16] D. Fologea, J. Uplinger, B. Thomas, D. S. McNabb, and J. Li, "Slowing DNA translocation in a solid-state nanopore," *Nano Lett.*, vol. 5, pp. 1734–1737, 2005.

[17] P. Chen, J. J. Gu, E. Brandin, Y. R. Kim, D. Wang, and D. Branton, "Probing single DNA molecule transport using fabricated nanopores," *Nano Lett.*, vol. 4, pp. 2293–2298, 2004.

[18] M. Gershow and J. A. Golovchenko, "Recapturing and trapping single molecules with a solid-state nanopore," *Nature Nanotech.*, vol. 2, pp. 775–779, 2007.

[19] M. Wanunu, J. Sutin, B. McNally, A. Chow, and A. Meller, "DNA translocation governed by interactions with solid-state nanopores," *Biophys. J.*, vol. 95, pp. 4716–4725, 2008.

[20] H. Chang, F. Kosari, G. Andreadakis, M. A. Alam, G. Vasmatzis, and R. Bashir, "DNA-mediated fluctuations in ionic current through silicon oxide nanopore channels," *Nano Lett.*, vol. 4, pp. 1551–1556, 2004.

[21] R. M. M. Smeets, U. F. Keyser, D. Krapf, M. Y. Wu, N. H. Dekker, and C. Dekker, "Salt dependence of ion transport and DNA translocation through solid-state nanopores," *Nano Lett.*, vol. 6, pp. 89–95, 2006.

[22] E. H. Trepagnier, A. Radenovic, D. Sivak, P. Geissler, and J. Liphardt, "Controlling DNA capture and propagation through artificial nanopores," *Nano Lett.*, vol. 7, pp. 2824–2830, 2007.

[23] D. Fologea, M. Gershow, B. Ledden, D. S. McNabb, J. A. Golovchenko, and J. Li, "Detecting single stranded DNA with a solid state nanopore," *Nano Lett.*, vol. 5, pp. 1905–1909, 2005.

[24] A. Han, G. Schurmann, G. Mondin, R. A. Bitterli, N. G. Hegelbach, N. F. de Rooij, and U. Staufer, "Sensing protein molecules using nanofabricated pores," *Appl. Phys. Lett.*, vol. 88, p. 093901, 2006.

[25] D. Fologea, B. Ledden, D. S. McNabb, and J. Li, "Electrical characterization of protein molecules in a solid-state nanopore," *Appl. Phys. Lett.*, vol. 91, p. 053901, 2007.

[26] R. Fan, R. Karnik, M. Yue, D. Li, A. Majumdar, and P. Yang, "DNA translocation in inorganic nanotubes," *Nano Lett.*, vol. 5, pp. 1633–1637, 2005.

[27] B. McNally, M. Wanunu, and A. Meller, "Electromechanical unzipping of individual DNA molecules using synthetic sub-2 nm pores," *Nano Lett.*, vol. 8, pp. 3418–3422, 2008.

[28] C. C. Harrell, Y. Choi, L. P. Horne, L. A. Baker, Z. S. Siwy, and C. R. Martin, "Resistive-pulse DNA detection with a conical nanopore sensor," *Langmuir*, vol. 22, pp. 10 837–10 843, 2006.

[29] H. Bayley, "Holes with an edge," *Nature*, vol. 467, pp. 164–165, 2010.

[30] G. F. Schneider, S. W. Kowalczyk, V. E. Calado, G. Pandraud, H. W. Zandbergen, L. M. Vandersypen, and C. Dekker, "DNA translocation through graphene nanopores," *Nano Lett.*, vol. 10, pp. 3163–3167, 2010.

[31] C. A. Merchant, K. Healy, M. Wanunu, V. Ray, N. Peterman, J. Bartel, M. D. Fischbein, K. Venta, Z. Luo, A. T. C. Johnson, and M. Drndić, "DNA translocation through graphene nanopores," *Nano Lett.*, vol. 10, pp. 2915–2921, 2010.

[32] S. Garaj, W. Hubbard, A. Reina, J. Kong, D. Branton, and J. A. Golovchenko, "Graphene as a subnanometre trans-electrode membrane," *Nature*, vol. 467, pp. 190–193, 2010.

[33] A. K. Geim, "Graphene: Status and prospects," *Science*, vol. 324, pp. 1530–1534, 2009.

[34] K. S. Novoselov, A. K. Geim, S. V. Morozov, D. Jiang, Y. Zhang, S. V. Dubonos, I. V. Grigorieva, and A. A. Firsov, "Electric field effect in atomically thin carbon films," *Science*, vol. 306, pp. 666–669, 2004.

[35] S. Garaj, S. Liu, J. A. Golovchenko, and D. Branton, "Molecule-hugging graphene nanopores," vol. 110, no. 30, pp. 12 192–12 196, 2013.

[36] H. W. C. Postma, "Rapid sequencing of individual dna molecules in graphene nanogaps," *Nano Lett.*, vol. 10, pp. 420–425, 2010.

[37] T. Thundat, "Read with quantum mechanics," *Nature Nanotech.*, vol. 5, pp. 246–247, 2010.

[38] T. Nelson, B. Zhang, and O. V. Prezhdo, "Detection of nucleic acids with graphene nanopores: Ab initio characterization of a novel sequencing device," *Nano Lett.*, vol. 10, pp. 3237–3242, 2010.

[39] J. Prasongkit, A. Grigoriev, B. Pathak, R. Ahuja, and R. H. Scheicher, "Transverse conductance of DNA nucleotides in a graphene nanogap from first principles," *Nano Lett.*, vol. 5, pp. 1941–1945, 2011.

[40] K. K. Saha, M. Drndić, and B. K. Nikolić, "DNA base-specific modulation of microampere transverse edge currents through a metallic graphene nanoribbon with a nanopore," *Nano Letters*, vol. 12, no. 1, pp. 50–55, 2012.

[41] S. M. Avdoshenko, D. Nozaki, C. Gomes da Rocha, J. W. Gonzàlez, M. H. Lee, R. Gutierrez, and G. Cuniberti, "Dynamic and electronic transport properties of DNA translocation through graphene nanopores," *Nano Letters*, vol. 13, no. 5, pp. 1969–1976, 2013.

[42] M. Puster, J. A. Rodríguez-Manzo, A. Balan, and M. Drndić, "Toward sensitive graphene nanoribbon-nanopore devices by preventing electron beam-induced damage," *ACS Nano*, vol. 7, no. 12, pp. 11 283–11 289, 2013.

[43] F. Traversi, C. Raillon, S. Benameur, K. Liu, S. Khlybov, M. Tosun, D. Krasnozhon, A. Kis, and A. Radenovic, "Detecting the translocation of DNA through a nanopore using graphene nanoribbons," *Nature Nanotech.*, vol. 8, no. 12, pp. 939–945, 2013.

[44] D. Lu, A. Aksimentiev, A. Y. Shih, E. Cruz-Chu, P. L. Freddolino, A. Arkhipov, and K. Schulten, "The role of molecular modeling in bionanotechnology," *Phys. Biol.*, vol. 3, pp. S40–S53, 2006.

[45] A. Aksimentiev, R. Brunner, J. Cohen, J. Comer, E. Cruz-Chu, D. Hardy, A. Rajan, A. Shih, G. Sigalov, Y. Yin, and K. Schulten, "Computer modeling in biotechnology, a partner in development," in *Protocols in Nanostructure Design*, ser. Methods in Molecular Biology. Humana Press, 2008, pp. 181–234.

[46] A. Aksimentiev and K. Schulten, "Imaging alpha-hemolysin with molecular dynamics: Ionic conductance, osmotic permeability and the electrostatic potential map," *Biophys. J.*, vol. 88, pp. 3745–3761, 2005.

[47] A. Aksimentiev, J. B. Heng, G. Timp, and K. Schulten, "Microscopic kinetics of dna translocation through synthetic nanopores," *Biophys. J.*, vol. 87, pp. 2086–2097, 2004.

[48] U. M. Mirsaidov, W. Timp, X. Zou, V. Dimitrov, K. Schulten, A. P. Feinberg, and G. Timp, "Nanoelectromechanics of methylated DNA in a synthetic nanopore," *Biophys. J.*, vol. 96, pp. L32–L34, 2009.

[49] J. C. Phillips, R. Braun, W. Wang, J. Gumbart, E. Tajkhorshid, E. Villa, C. Chipot, R. D. Skeel, L. Kale, and K. Schulten, "Scalable molecular dynamics with NAMD," *J. Comp. Chem.*, vol. 26, pp. 1781–1802, 2005.

[50] X.-J. Lu and W. K. Olson, "3DNA: A software package for the analysis, rebuilding and visualization of three-dimensional nucleic acid structures," *Nucleic Acids Res.*, vol. 31, pp. 5108–5121, 2003.

[51] A. D. MacKerell, Jr., D. Bashford, M. Bellott, R. L. Dunbrack, Jr., J. D. Evanseck, M. J. Field, S. Fischer, J. Gao, H. Guo, S. Ha, D. Joseph, L. Kuchnir, K. Kuczera, F. T. K. Lau, C. Mattos, S. Michnick, T. Ngo, D. T. Nguyen, B. Prodhom, I. W. E. Reiher, B. Roux, M. Schlenkrich, J. Smith, R. Stote, J. Straub, M. Watanabe, J. Wiorkiewicz-Kuczera, D. Yin, and M. Karplus, "All-atom empirical potential for molecular modeling and dynamics studies of proteins." *J. Phys. Chem. B*, vol. 102, pp. 3586–3616, 1998.

[52] D. Lu, Y. Li, U. Ravaioli, and K. Schulten, "Empirical nanotube model for biological applications," *J. Phys. Chem. B*, vol. 109, pp. 11 461–11 467, 2005.

[53] W. L. Jorgensen, J. Chandrasekhar, J. D. Madura, R. W. Impey, and M. L. Klein, "Comparison of simple potential functions for simulating liquid water," *J. Chem. Phys.*, vol. 79, no. 2, pp. 926–935, 1983.

[54] G. J. Martyna, D. J. Tobias, and M. L. Klein, "Constant pressure molecular dynamics algorithms," *J. Chem. Phys.*, vol. 101, no. 5, pp. 4177–4189, 1994.

[55] W. Humphrey, A. Dalke, and K. Schulten, "VMD – Visual Molecular Dynamics," *J. Mol. Graphics*, vol. 14, pp. 33–38, 1996.

[56] M. Wanunu, W. Morrison, Y. Rabin, A. Y. Gorsberg, and A. Meller, "Electrostatic focusing of unlabelled DNA into nanoscale pores using a salt gradient," *Nature Nanotech.*, vol. 5, pp. 160–165, 2009.

[57] M. Muthukumar, "Theory of capture rate in polymer translocation," *J. Chem. Phys.*, vol. 132, pp. 195 101(1–10), 2010.

[58] A. Y. Grosberg and Y. Rabin, "DNA capture into a nanopore: Interplay of diffusion and electrohydrodynamics," *J. Chem. Phys.*, vol. 133, pp. 1 651 021(1–15), 2010.

[59] J. Li, M. Gershow, D. Stein, E. Brandin, and J. A. Golovchenko, "DNA molecules and configurations in a solid-state nanopore microscope," *Nat. Mater.*, vol. 2, pp. 611–615, 2003.

[60] S. V. Dorp, U. F. Keyser, N. H. Dekker, C. Dekker, and S. G. Lemay, "Origin of the electrophoretic force on DNA in solid-state nanopores," *Nature Phys.*, vol. 5, pp. 347–351, 2009.

[61] P. Chen, J. Gu, E. Brandin, Y.-R. Kim, Q. Wang, and D. Branton, "Probing single DNA molecule transport using fabricated nanopores," *Nano Lett.*, vol. 4, pp. 2293–2298, 2004.

[62] B. Luan and A. Aksimentiev, "Control and reversal of the electrophoretic force on DNA in a charged nanopore," *J. Phys.: Condens. Matter*, vol. 22, p. 454123, 2010.

[63] A. Meller, L. Nivon, E. Brandin, J. Golovchenko, and D. Branton, "Rapid nanopore discrimination between single polynucleotide molecules," *Proc. Natl. Acad. Sci. USA*, vol. 97, pp. 1079–1084, 2000.

[64] S. Howorka, S. Cheley, and H. Bayley, "Sequence-specific detection of individual DNA strands using engineered nanopores," *Nat. Biotechnol.*, vol. 19, pp. 636–639, 2001.

[65] A. Meller and D. Branton, "Single molecule measurements of DNA transport through a nanopore," *Electrophoresis*, vol. 23, pp. 2583–2591, 2002.

[66] D. Deamer and D. Branton, "Characterization of nucleic acids by nanopore analysis," *Acc. Chem. Res.*, vol. 35, pp. 817–825, 2002.

[67] Z. S. Siwy and M. Davenport, "Graphene opens up to DNA," *Nature Nanotech.*, vol. 5, pp. 697–698, 2010.

[68] K. Sint, B. Wang, and P. Kŕal, "Selective ion passage through functionalized graphene nanopores," *J. Am. Chem. Soc.*, vol. 130, pp. 16 448–16 449, 2008.

[69] G. Sigalov, J. Comer, G. Timp, and A. Aksimentiev, "Detection of DNA sequences using an alternating electric field in a nanopore capacitor," *Nano Lett.*, vol. 8, pp. 56–63, 2007.

[70] B. Dorvel, G. Sigalov, Q. Zhao, J. Comer, V. Dimitrov, U. Mirsaidov, A. Aksimentiev, and G. Timp, "Analyzing the forces binding a restriction endonuclease to DNA using a synthetic nanopore," *Nucleic Acids Res.*, vol. 37, pp. 4170–4179, 2009.

[71] D. Lu, Y. Li, U. Ravaioli, and K. Schulten, "Ion-nanotube terahertz oscillator," *Phys. Rev. Lett.*, vol. 95, p. 246801, 2005.

[72] Y. Zhang, T. Tang, C. Girit, Z. Hao, M. Martin, A. Zettl, M. F. Crommie, Y. R. Shen, and F. Weng, "Direct observation of a widely tunable bandgap in bilayer graphene," *Nature*, vol. 459, pp. 820–823, 2009.

[73] Y. He, R. Scheicher, A. Grigoriev, R. Ahuja, S. Long, Z. Huo, and M. Liu, "2010 10th IEEE international conference on solid-state and Integrated Circuit Technology (ICSICT)," Nov. 2010, pp. 1483–1485.

[74] A. Geim and K. S. Novoselov, "The rise of graphene," *Nat. Methods*, vol. 6, pp. 183–191, 2007.

[75] K. Novoselov, E. Mccann, S. Morozov, V. Fal'ko, M. katsnelson, U. Zeitler, D. Jiang, F. Schedin, and A. Geim, "Unconventional quantum Hall effect and Berry's phase of 2π in bilayer graphene," *Nature Phys.*, vol. 2, pp. 177–180, 2006.

[76] B. M. Venkatesan and R. Bashir, "Nanopore sensors for nucleic acid analysis," *Nature Nanotech.*, no. 10, pp. 615–624, 10 2011.

[77] A. H. Castro Neto, F. Guinea, N. M. R. Peres, K. S. Novoselov, and A. K. Geim, "The electronic properties of graphene," *Rev. Mod. Phys.*, vol. 81, pp. 109–162, Jan 2009.

[78] F. Cervantes-Sodi, G. Csányi, S. Piscanec, and A. C. Ferrari, "Edge-functionalized and substitutionally doped graphene nanoribbons: Electronic and spin properties," *Phys. Rev. B*, vol. 77, p. 165427, Apr 2008.

[79] K. A. Ritter and J. W. Lyding, *Nature Materials*, vol. 8, no. 3, pp. 235–242, 2009.

[80] W. H. Press, S. A. Teukolsky, W. T. Vetterling, and B. P. Flannery, *Numerical Recipes in C: The Art of Scientific Computing*. New York, NY, USA: Cambridge University Press, 1992.

[81] T. B. Boykin, M. Luisier, G. Klimeck, X. Jiang, N. Kharche, Y. Zhou, and S. K. Nayak, "Accurate six-band nearest-neighbor tight-binding model for the π-bands of bulk graphene and graphene nanoribbons," *Journal of Applied Physics*, vol. 109, no. 10, 2011.

[82] S. Datta, *Quantum Transport: Atom to Transistor*. Cambridge University Press, 2013.

[83] S. Banerjee, J. Shim, J. Rivera, X. Jin, D. Estrada, V. Solovyeva, X. You, J. Pak, E. Pop, N. Aluru, and R. Bashir, "Electrochemistry at the edge of a single graphene layer in a nanopore," *ACS Nano*, vol. 7, no. 1, pp. 834–843, 2013.

[84] J. Bath and A. J. Turberfield, "DNA nanomachines," *Nature Nanotech.*, vol. 2, pp. 275–84, 2007.

[85] M. Rief, H. Clausen-Schaumann, and H. E. Gaub, "Sequence-dependent mechanics of single DNA molecules," *Nat. Struct. Biol.*, vol. 6, pp. 346–349, 1999.

[86] C. Ke, M. Humeniuk, H. S-Gracz, and P. E. Marszalek, "Direct measurements of base stacking interactions in DNA by single-molecule atomic-force spectroscopy," *Phys. Rev. Lett.*, vol. 99, p. 018302, 2007.

[87] H. Clausen-Schaumann, M. Rief, C. Tolksdorf, and H. E. Gaub, "Mechanical stability of single DNA molecules," *Biophys. J.*, vol. 78, no. 4, pp. 1997–2007, 2000.

[88] S. B. Smith, L. Finzi, and C. Bustamante, "Direct mechanical measurements of the elasticity of single DNA molecules by using magnetic beads," *Science*, vol. 258, pp. 1122–1126, 1992.

[89] S. B. Smith, Y. Cui, and C. Bustamante, "Overstretching B-DNA: The elastic response of individual double-stranded and single-stranded DNA molecules," *Science*, vol. 271, pp. 795–799, 1996.

[90] U. F. Keyser, B. N. Koeleman, S. Van Dorp, D. Krapf, R. M. Smeets, S. G. Lemay, N. H. Dekker, and C. Dekker, "Direct force measurements on DNA in a solid-state nanopore," *Nature Physics*, vol. 2, no. 7, pp. 473–477, 2006.

[91] D. V. Melnikov, J.-P. Leburton, and M. E. Gracheva, "Slowing down and stretching dna with an electrically tunable nanopore in a p-n semiconductor membrane," *Nanotechnology*, vol. 23, p. 255501, 2012.

[92] P. Cluzel, A. Lebrun, C. Heller, R. Lavery, J.-L. Viovy, D. Chatenay, and F. Caron, "DNA: An extensible molecule," *Science*, vol. 271, pp. 792–794, 1996.

[93] R. Lohikoski, J. Timonen, and A. Laaksonen, "Molecular dynamics simulation of single DNA stretching reveals a novel structure," *Chemical Physics Letters*, vol. 407, pp. 23–29, 2005.

[94] A. Balaeff, S. L. Craig, and D. N. Beratan, "B-DNA to zip-DNA: Simulating a DNA transition to a novel structure with enhanced charge-transport characteristics," *The Journal of Physical Chemistry A*, vol. 115, no. 34, pp. 9377–9391, 2011.

[95] H. Grubmüller, H. Heller, A. Windemuth, and K. Schulten, "Generalized Verlet algorithm for efficient molecular dynamics simulations with long-range interactions," *Mol. Sim.*, vol. 6, pp. 121–142, 1991.

[96] T. Schlick, R. Skeel, A. Brünger, L. Kalé, J. A. Board Jr., J. Hermans, and K. Schulten, "Algorithmic challenges in computational molecular biophysics," *J. Comp. Phys.*, vol. 151, pp. 9–48, 1999.

[97] H. C. Andersen, "Rattle: A 'velocity' version of the shake algorithm for molecular dynamics calculations," *J. Chem. Phys.*, vol. 52, pp. 24–34, 1983.

[98] S. Miyamoto and P. A. Kollman, "SETTLE: An analytical version of the SHAKE and RATTLE algorithm for rigid water molecules," *J. Comp. Chem.*, vol. 13, no. 8, pp. 952–962, 1992.

[99] E. H. Hwang and S. Das Sarma, "Dielectric function, screening, and plasmons in two-dimensional graphene," *Phys. Rev. B*, vol. 75, p. 205418, 2007.

[100] A. Girdhar, C. Sathe, K. Schulten, and J.-P. Leburton, "Gate-modulated graphene quantum point contact device for DNA sensing," 2014, submitted.

[101] M. Sotomayor and K. Schulten, "Single-molecule experiments in vitro and in silico," *Science*, vol. 316, pp. 1144–1148, 2007.

[102] E. H. Lee, J. Hsin, M. Sotomayor, G. Comellas, and K. Schulten, "Discovery through the computational microscope," *Structure*, vol. 17, pp. 1295–1306, 2009.

[103] M. Santosh and P. K. Maiti, "Force induced DNA melting," *Journal of Physics: Condensed Matter*, vol. 21, no. 3, p. 034113, 2009.

[104] A. Lebrun and R. Lavery, "Modelling extreme stretching of DNA," *Nucl. Acids Res.*, vol. 24, no. 12, pp. 2260–2267, 1996.

[105] S. A. Harris, Z. A. Sands, and C. A. Laughton, "Molecular dynamics simulations of duplex stretching reveal the importance of entropy in determining the biomechanical properties of DNA," *Biophysical Journal*, vol. 88, no. 3, pp. 1684–1691, 2005.

[106] B. Luan and A. Aksimentiev, "Strain softening in stretched DNA," *Phys. Rev. Lett.*, vol. 101, p. 118101, Sep 2008.

[107] P. M. Severin, X. Zou, H. E. Gaub, and K. Schulten, "Cytosine methylation alters DNA mechanical properties," *Nucleic Acids Res.*, vol. 39, pp. 8740–8751, 2011.

[108] P. M. Severin, X. Zou, K. Schulten, and H. E. Gaub, "Effects of cytosine hydroxymethylation on DNA strand separation," *Biophys. J.*, vol. 104, pp. 208–215, 2013.

[109] B. Isralewitz, M. Gao, and K. Schulten, "Steered molecular dynamics and mechanical functions of proteins," *Curr. Opin. Struct. Biol.*, vol. 11, pp. 224–230, 2001.

[110] M. Gao, M. Sotomayor, E. Villa, E. Lee, and K. Schulten, "Molecular mechanisms of cellular mechanics," *Phys. Chem. Chem. Phys.*, vol. 8, pp. 3692–3706, 2006.

[111] A. Girdhar, C. Sathe, K. Schulten, and J.-P. Leburton, "Graphene quantum point contact transistor for DNA sensing," *Proc. Natl. Acad. Sci. USA*, vol. 110, pp. 16 748–16 753, 2013.